약학박사학위논문

Pathophysiological roles of Anoctamin 1 in the development of benign prostatic hyperplasia

전립선 비대증에서 Anoctamin1의 병태생리학적 기능 연구

2015년 8월

서울대학교 대학원

분자의학 및 바이오제약학과

분자의학 및 바이오제약학 전공

차 주 영

Pathophysiological roles of Anoctamin 1 in the development of benign prostatic hyperplasia

전립선 비대증에서 Anoctamin1의 병태생리학적 기능 연구

지도교수 오 우 택

이 논문을 약학박사 학위논문으로 제출함

2015년 8월

서울대학교 대학원

분자의학 및 바이오제약학과

분자의학 및 바이오제약학 전공

차 주 영

차주영의 박사학위논문을 인준함

2015년 8월

위 원 장 _____ (인)

부 위 원 장 _____ (인)

위 원 _____ (인)

위 원 _____ (인)

위 원 _____ (인)

Abstract

Benign prostate hyperplasia (BPH) is characterized by enlargement of the prostate, causing lower urinary tract symptoms in elderly men worldwide. However, the molecular mechanism underlying the pathogenesis of BPH is unclear. Anoctamin1 (ANO1) encodes a Ca2+-activated chloride channel (CaCC) that mediates various physiological functions. Here we demonstrate that it is essential for testosterone-induced BPH. ANO1 was highly amplified in dihydrotestosterone (DHT)-treated prostate epithelial cells, whereas the selective knockdown of ANO1 inhibited DHT-induced cell proliferation. Three androgen-response elements were found in the ANO1 promoter region, which were relevant for the DHT-dependent induction of ANO1. Administration of an ANO1 blocker or Ano1 small interfering RNA inhibited prostate enlargement and reduced histological abnormalities in vivo. We therefore concluded that ANO1

is essential for the development of prostate hyperplasia and is a potential target for the treatment of BPH.

Keywords: Anoctamin 1 (ANO1), benign prostate hyperplasia (BPH), proliferation

Student Number: 2011-31342

Table of Contents

List of Figures

List of Table

Introduction

1. Chloride Channel

1.1 Overview

Chloride channels play a pivotal role in numerous functions both in normal and disease state of human body by modulating trans-epithelial fluid transport, cell-volume, muscle contraction, sensory transduction, neuronal excitability, blood pressure, cell cycle, and apoptosis. Especially, within cells, chloride transport across organellar membranes is involved in endosomal, lysosomal and Golgi acidification. Chloride channels provide the major route for transmembrane chloride transport in these processes (1).

In addition, various genetic diseases, such as cystic fibrosis, nephrolithiasis, Bartter's syndrome, kidney disorders, and neurodegenerative disease are also caused by mutations in chloride channels (2-5). Among them, the most well known disease is cystic fibrosis, which is caused by mutation of cystic fibrosis transmembrane conductance regulator

(CFTR) gene, has prevalence of 1 in 2,000 Caucasians (6, 7).

1.2 Classification of Chloride Channels

Mammalian chloride channels are divided into five classes based on their regulation mechanism: voltage-gated chloride channels (ClCs), CFTR, ligand-gated chloride channels (GABA (gamma-aminobutyric acid)-, glycine-activated), volume-regulated chloride channels (VRAC), and calcium-activated chloride channels (CaCCs).

1.2.1 ClC Channels

The ClC chloride channels family was firstly identified as voltage-gated Chloride channel (ClC-0) from the marine electric ray *Torpedo marmorata* (8). The ClC family comprises nine homologs and is categorized into three subfamilies based on their gene sequences (9). ClC-0 and its mammalian homologues, ClC-1, ClC-2, ClC-Ka, and ClC-Kb, share 50–60% sequence identity among each other. These channels are all present on the cell membrane to control the Cl^- flux and the membrane potential, and therefore are grouped together in the subfamily called muscle-type ClC channels. The second branch of the family includes ClC-3, ClC-4, and ClC-

5. These channels were recently found to be located on the membrane of intracellular vesicles and are thought to be important in maintaining the pH of these vesicles (10). The third subfamily comprises ClC-6 and ClC-7, which are broadly expressed in various tissues. They may be present also in the intracellular organelles to regulate the vesicular pH (11, 12). Most recent analysis of transport mechanisms of human CLC isoforms demonstrated that five out of nine human CLCs (ClC-3 through ClC-7), displayed anion-proton exchangers rather than anion channels (13, 14).

ClC channels have many physiological roles, including maintenance of membrane potential, regulation of transepithelial Cl^- transport, and control of intravesicular pH. The physiological importance of these channels is best illustrated by the hereditary diseases caused by defects of these channels, such as congenital myotonia (15), Dent's disease (16), Bartter's syndrome (17), and idiopathic epilepsy (18).

1.2.2 Cystic Fibrosis Transmembrane Regulator

CFTR has pivotal role in Cl^- secretion in apical membrane of various epithelia cells from intestine, airways, glands, bile duct, pancreas, and liver (19-21). This channel belongs to the superfamily of ABC transporter

ATPases (2). Cystic fibrosis (CF) is caused by mutations in the gene that encodes CFTR protein (7, 22). Absence or defective function of CFTR protein product is directly or indirectly responsible for disease pathogenesis in CF-affected organs. The manifestations of CF generally arise when ductal or glandular obstruction occurs due to an inability to hydrate macromolecules within affected ductal lumens. The CFTR protein functions on the apical surface of epithelial cells as a cyclic AMP-dependent chloride channel, a bicarbonate channel and as a modulator of other ion channels (23-25).

1.2.3 GABA/glycine Receptors

Ionotropic GABA and glycine receptors play a pivotal role in inhibitory synaptic transmission in the brain and spinal cord, respectively. All GABA- and glycine-activated chloride channels form with pentameric proteins by assembling different subunits. In case of glycine receptors, there are four types of alpha subunit (alpha1–4) and one type of beta subunit. GABAA receptors are typically formed by the assembly of two alpha, two beta and one gamma subunit. Currently, eleven native GABAA receptors are classed as conclusively identified (i.e., a1b2g2, a1bg2, a3bg2, a4bg2, a4b2d, a4b3d, a5bg2, a6bg2, a6b2d, a6b3d and r) with further receptor isoforms

occurring with high probability, or only tentatively (26). The inhibitory function of GABA and glycine receptors is a consequence of the electrochemical potential for chloride. In the postsynaptic membrane, opening of GABA- or glycine-activated chloride channels triggers chloride influx and membrane hyperpolarization, inhibiting excitability (27, 28). Pharmacologically, the potency and efficacy of many GABA agonists varies between GABAA receptor isoforms. The antagonists - bicuculline and gabazine - differ in their inhibitory potency to suppress spontaneous openings of the GABAA receptor, the former being more effective (29).

1.2.4 Calcium-activated Chloride Channel

Calcium-activated chloride channel is described in chapter 1.3 in detail.

1.3 Calcium-activated Chloride Channel

In the early 1980's, Ca^{2+}-activated Cl^- channels (CaCCs) were first described in Xenopus oocytes and salamander rods (30, 31). CaCCs are broadly expressed in various organs and play important roles in cell physiology including epithelial secretion (32, 33), sensory transduction and adaptation (34-38), regulation of smooth muscle contraction (39), control of

neuronal and cardiac excitability (40), and nociception (41).

1.3.1 Physiological Role of CaCCs

1.3.1.1 Fluid Secretion by Exocrine Glands

Intestinal epithelium secretes Cl^- into the lumen of intestine transiently by Ca^{2+} elevating agonists such as carbachol, histamine and nucleotides. Airway epithelia also secrete fluid into the airway. Acinar and duct cells from lachrymal, parotid, submandibular, and sublingual glands, as well as pancreas secrete isotonic plasma like primary fluid that is rich in NaCl. The fluid secretion is Ca^{2+} dependent and triggered by the parasympathetic neurotransmitter acetylcholine (42, 43). The rise in $[Ca^{2+}]i$ is triggered by the muscarinic receptor induces production of IP3 which releases Ca^{2+} from internal stores. The elevation of $[Ca^{2+}]i$ activates CaCCs and subsequently a Cl^- efflux through the apical membrane. The exit of Cl^- drives the movement of Na^+ through the parallel pathway and drags water, resulting in salty fluid secretion. Thus CaCCs are central to the fluid secretion process because they constitute the last step in the transepithelial movement of Cl^-, which is the net driving force for the whole process.

1.3.1.2 Smooth Muscle Contraction

CaCCs have been extensively studied in smooth muscle cells derived from a variety of tissues and appear to be involved in both regulation of myogenic tone and contraction stimulated by agonists (44). Activation of CaCCs in smooth muscle can occur by Ca^{2+} entry through VGCCs or by Ca^{2+} release from intracellular stores by inositol 1,4,5-triphosphate (IP3) generated through the phospholipase C (PLC) pathway. Because E_{Cl} is positive to the resting potential in smooth muscle, opening CaCCs will produce a depolarization (44).

1.3.1.3 Regulation of Cardiac Excitability

In some species, CaCCs play a role in repolarization of the cardiac action potential. In many cardiac myocytes, the transient outward currents Ito2 and Ito1 are responsible for the initial phase of repolarization. Ito1 is a Ca^{2+}-insensitive K^+ current blocked by 4-aminopyridine, and Ito2 is a Cl^- current stimulated by Ca^{2+} but insensitive to 4-aminopyridine (39, 44). The state of Ca^{2+} buffering plays a key role in determining the relative contribution of CaCCs to the total transient outward current.

1.3.1.4 Kidney

CaCCs are largely expressed in kidney, such as rabbit distal convoluted tubule, proximal convoluted tubule, and cortical collecting duct. Moreover, intramedullary collecting duct (IMCD) cell lines like IMCD-K2 and IMCD-K3 which acutely isolated from IMCD also showed high level of CaCC expression (45). There is also growing knowledge that fluid and salt secretion in the distal kidney may contribute to urine composition (46). In the IMCD, for example, there is good evidence that Cl^- secretion occurs by both CaCCs and CFTR (47).

1.3.1.5 Endothelial Cells

Endothelial cells are involved in preventing blood clotting, immune responses, and angiogenesis and produce a variety of vasoactive substances, including NO, prostaglandins, and endothelins. Humoral substances and flow rate can also be sensed by endothelial cells. Agonists such as histamine, ATP, and thrombin increase $[Ca^{2+}]$i-dependent Cl^- fluxes and Cl^- currents by activation of CaCCs in endothelial cells (48, 49). CaCCs have been implicated in the control of the membrane potential that would help to maintain the driving force for Ca^{2+}. They could also play a role in the

control of cell volume and cell proliferation (50, 51).

1.3.2 Mechanism of Activation

The Ca^{2+} that activates CaCCs can come from either Ca^{2+} influx or Ca^{2+} release from intracellular stores. In some cases, it has been documented that specific types of ion channels are coupled to CaCCs. There are two possible general mechanisms for Ca^{2+} to activate CaCCs: Ca^{2+} could bind directly to the channel protein or act indirectly on the channel via Ca^{2+}-binding proteins or Ca^{2+}-dependent enzymes.

2. TMEM 16 Family

2.1 Overview

In 2008, three independent research teams found the orphan proteins, TMEM16A, is a component of the Ca^{2+}-activated Cl^- channel, CaCC (52-54). These are two members of a family that consists of 10 genes in mammals (55). Yang et al proposed the new name “anoctamin” or ANO (Anion + Octa = 8) and this name is now approved by the official HUGO

nomenclature committee and has replaced TMEM16 in Genbank. TMEM16A is now ANO1, TMEM16B is ANO2, and so-on except that the letter I was skipped in the TMEM16 nomenclature so that TMEM16J is ANO9 and TMEM16K is ANO10. This type of Cl^- channel had been known at the functional level for more than 25 years, but there was no clear understanding of its molecular identity (56). Typical features of this channel are as follows: 1) outward rectification of the steady-state current-voltage relationship due to activation and deactivation at positive and negative membrane potentials, respectively; and 2) activation by cytosolic Ca^{2+} with an apparent affinity that is increased by a change of the membrane potential to positive values. CaCC activity may be detected with a series of techniques including patch-clamp, short-circuit current recordings, and fluorescent measurements of I^-/Cl^- fluxes (57). Several groups followed this breakthrough discovery by confirming these initial findings and expanded the breadth of physiological processes regulated by Ca^{2+}-activated Cl^- currents mediated by ANO1 and ANO2 that are as diverse as nociception, epithelial secretion, neuronal signaling, smooth muscle contraction, host defense, cell proliferation, signal transduction and tumorigenesis (58-64). Even though these advances greatly expanded our knowledge of the physiological roles of CaCCs, our insights into the molecular bases of Ca^{2+}-dependent Cl^- transport by Anoctamin proteins remain extremely limited

because of the lack of information on even their most basic structural features, such as their topological organization, and the localization of the ion conduction pore (65-67).

2.2 Topology of the TMEM16 Proteins

TMEM16 proteins can also be studied after purification and reconstitution in artificial membranes. Hydropathy analysis shows that all TMEM16s have eight hydrophobic helices that are likely to be transmembrane domains (TM) with cytosolic N- and C-termini. However, more investigation is required to establish the topology of these proteins. The Anoctamin family comprises ~ 1400 sequences divided in 10 different clades and its members are found only in eukaryotes. Several lines of evidence suggest that Anoctamins form homodimers (68-70), but the possibility of heterodimer formation has not been investigated in depth. The topology of Anoctamin homologues is still unclear and three competing models have been proposed (67, 71). The cytosolic localization of the N- and C-termini implies that the Anoctamins have an even number of TM segments, with most programs predicting that the TMEM16s have eight TMs (52, 67). The precise identification of the boundaries of these regions is uncertain as different programs identify variable numbers of TM regions

with different boundaries (67). The degree of homology between Anoctamins from the same clade is higher and decreases between different clades. The evolutionarily conserved stretches are likely to underlie common mechanistic features of the family, such as the Ca^{2+} binding site. Indeed, one of the better preserved regions, between residues 700 and 760, contains amino acids important for Ca^{2+} (68, 72), which appears to be one of the more conserved features among Anoctamins. Most recently, it was reported that the Ca^{2+} sensor helix attaches to the reference helix in the resting state, and as intracellular Ca^{2+} rises, Ca^{2+} acts on the sensor helix, which repels it from the reference helix. This Ca^{2+}-dependent push-pull conformational change would be a key electromechanical movement for gating the ANO1 channel (66). In contrast, the location of the ion permeation pathway of Anoctamin channels remains poorly defined, mostly because of the poor sequence conservation and difficulty in defining the TM domains in the absence of direct structural information.

2.3 Pathophysiological Functions of Anoctamin Paralogues

2.3.1 ANO1

ANO1 is widely expressed in secretory epithelium, such as salivary

gland, pancreas, gut, mammary gland, and airway epithelium (52, 53, 59, 73). ANO1 knockout mice show malfunction of Ca^{2+}-dependent Cl^- secretion in various epithelia (74-76) and ANO1 has been applied in rotovirus-induced diarrhea (77). Moreover, ANO1 is expressed in a variety of other cell types including certain smooth muscles and sensory neurons. ANO1 is a secondary Cl^- channel in airway. The major Cl^- channel in human airway is CFTR. CaCCs have long been considered as a potential target for therapy of cystic fibrosis based on the idea that upregulation or activation of CaCCs might compensate for loss of CFTR in airway fluid secretion. Recently, however, Namkung et al (57) showed that novel ANO1 inhibitors were rather ineffective in inhibiting CaCCs in airway epithelial cells despite their efficacy in inhibiting heterologously expressed ANO1 as well as native CaCCs in salivary gland. This result does not match with the several reports that ANO1 is expressed in airway epithelium and that knockout of ANO1 decreases airway secretion (59, 74, 75). In addition to airway, cystic fibrosis affects other tissues - reproductive tract, pancreas, and bile duct. ANO1 is expressed in all of these tissues and may be an alternative, non-CFTR Cl^- secretory pathway (59, 78).

2.3.2 ANO2

ANO2 plays an important role in sensory transduction in olfactory sensory neurons (35). Ca^{2+} influx through the cyclic nucleotide gated channels then activates CaCCs that amplify the receptor potential. It seems ANO2 is the best candidate for the pore-forming subunit of CaCCs in olfactory sensory neurons (34, 79). ANO2 generates Ca^{2+}-activated chloride currents when expressed in heterologous systems (54, 80). ANO2 is localized in the cilia and dendritic knobs of olfactory sensory neurons and displays electrophysiological properties similar to native olfactory CaCCs. ANO2 displays similar halide permeability, Ca^{2+} sensitivity, single-channel conductance, and rundown kinetics to native olfactory CaCCs (34). However, there are differences in channel inactivation kinetics, suggesting the possible presence of other regulatory subunits. In addition, ANO2 is highly expressed in photoreceptor synaptic terminals (38). ANO2 is localized to presynaptic membranes in ribbon synapses, where it co-localizes with the adapter proteins PSD95, MPP4, and VELI3. ANO1 has also been shown to be expressed in photoreceptor terminals, suggesting there may be a contribution by both proteins to CaCCs in photoreceptors (81).

2.3.3 ANO6

Recently, ANO6 mutations have been reported in Scott syndrome, a rare congenital bleeding disorder caused by a defect in blood coagulation (82). In platelets, like other cell types, phosphatidylserine is located on the inner leaflet of the plasma membrane. When platelets are activated they expose phosphatidylserine on the outer leaflet of the plasma membrane to promote clotting. This redistribution of phosphatidylserine is mediated by phospholipid scramblases that transport phospholipids bi-directionally from one leaflet to the other. In patients with Scott syndrome this mechanism is defective, resulting in impaired blood clotting. Ano6 was found to be critical for Ca^{2+} dependent exposure of phosphatidylserine on the cell surface in Ba/F3 platelet cells. Furthermore, a patient with Scott syndrome harbored a mutation at a splice-acceptor site of ANO6, resulting in premature termination of the protein. Cells derived from this patient did not expose phosphatidylserine in response to a Ca^{2+} ionophore, unlike cells derived from the patient's unaffected parents. These data imply that ANO6 is required for scramblase activity.

2.3.4 ANO7

Of 40,000 human genes examined, 8 novel genes, including ANO7, were identified as being the most closely linked to known prostate cancer genes (83, 84). ANO7 is expressed on the apical and lateral membranes of normal prostate. In the prostate LnCap cell line stably transfected with ANO7, the protein localizes to cell-cell contact regions. It has been suggested that Ano7 promotes cell association because cell association can be reduced with RNAi targeted to ANO7 (84). Predominant expression in prostate and prostate cancer poises ANO7 as an attractive candidate for immunotherapy (85, 86), although the role of ANO7 in the development of prostate cancer is elusive.

2.3.5 ANO10

Ataxia mutations in ANO10 have been linked to autosomal recessive cerebellar ataxias associated with moderate gait ataxia, downbeat nystagmus, and dysarthric speech (87-89). Affected individuals display severe cerebellar atrophy. Two of the mutations introduce premature stop codons, probably leading to null protein expression. Most recent study demonstrated that a coding variant of ANO10 affects volume regulation of macrophage (90).

However, it remains uncertain whether ANO10 is an ion channel, because ANO10 and ANO8 constitute the most divergent branch of the anoctamin family.

2.6. Role of ANO1 in cell proliferation

Originally, ANO1 has been recognized by several other names including DOG1 (Discovered On GIST-1 tumor), ORAOV2 (Oral cancer Overexpressed), and TAOS-2 (Tumor Amplified and Overexpressed) and attracted the interest of cancer biologists since it is upregulated in various cancer types (91-94). Gene expression profiling identified Ano1 was highly expressed in gastrointestinal stromal tumors (GISTs), oral cancer, and head and neck squamous cell carcinomas. In addition, amplification of the Ano1 locus is correlated with a poor prognosis (95, 96). Ano1 expression is also significantly increased in patients with a propensity to develop metastases. Given the role that Cl^- channels play in cell proliferation and migration, it is conceivable that Ano1 overexpression provides a growth or metastatic advantage to cancer cells (97). Supporting the role of Ano1 in metastasis is that overexpression of Ano1 stimulates cell movement. In contrast, silencing of Ano1 decreases cell migration; treatment of cells with CaCC blockers has a similar effect.

3. Benign prostatic hyperplasia

3.1 Signs and symptoms

Benign prostatic hyperplasia (BPH) is a pathological condition characterized by nonmalignant enlargement of the prostate gland, common in elderly men (98). Patients with BPH typically present with lower urinary tract symptoms (LUTS), which can be classified as either urinary tract obstructive symptoms such as hesitancy, intermittent stream and straining, or urinary bladder irritation symptoms such as frequency, urgency and urge incontinence. Urinary retention, whether acute or chronic, is also common (99).

3.2 Etiology

The precise molecular etiology of BPH is uncertain. The observed increase in cell number may be because of epithelial and stromal proliferation or of impaired programmed cell death or apoptosis leading to cellular accumulation. Androgens, estrogens, stromal–epithelial interactions, growth factors and neurotransmitters may play a role, either singly or in combination, in the etiology of the hyperplastic process (100).

3.3 Pathophysiology

The pathophysiology of BPH remains unclear. The development of the histologic features of BPH is dependent on the level of testosterone and DHT (101). According to the previous reports, castration in a man results in glandular atrophy and regression of lower urinary tract symptoms and a congenital lack of 5α-reductase leads to a vestigial prostate gland (102, 103). Moreover, other physiological markers associated with an increased risk of BPH include high levels of estradiol, insulin like growth factors (IGFs), and inflammatory markers (104-107). However, mechanisms underlying these associations remain poorly understood. Histologically, BPH is characterized by hyperplasia of both epithelial and stromal tissues within the prostate gland. Histological hyperplasia of the prostate is commonly observed in older men, so that some urologists and researchers consider it a natural occurrence during the process of prostate development and aging.

3.4 Diagnosis

Rectal examination (palpation of the prostate through the rectum) may reveal a markedly enlarged prostate, usually affecting the middle lobe (108, 109). Often, blood tests are performed to rule out prostatic malignancy:

elevated prostate specific antigen (PSA) levels needs further investigations such as reinterpretation of PSA results, in terms of PSA density and PSA free percentage, rectal examination and transrectal ultrasonography (110). These combined measures can provide early detection. Ultrasound examination of the testicles, prostate, and kidneys is often performed, again to rule out malignancy and hydronephrosis (111). Screening and diagnostic procedures for BPH are similar to those used for prostate cancer.

3.5 Epidemiology

About half of the male population over the age of 50 can be diagnosed with histological BPH, and this prevalence increases with age to about 90% over the age of 80 (98). Incidence rates of BPH increase from 3 cases per 1000 man-years at age 45–49 years, to 38 cases per 1000 man-years by the age of 75–79 years. While the prevalence rate is 2.7% for men aged 45–49, it increases to 24% by the age of 80 years (112). Globally, about 210 million males as of 2010 (6% of the population) are suffered by BPH.

3.6 Therapeutics

Medical management of BPH and LUTS typically involves the

reduction of prostate size by hormonal treatment, adrenergic blockade of urinary bladder tone or both. The current medical treatment of BPH includes two general classes of drugs namely the α-blockers and the 5α-reductase inhibitors (5-ARIs), either as monotherapy or as combination in specific clinical situations (99, 113). Since the male prostate and urethra contain α1-adrenergic receptors, α-blockers theoretically act by antagonising the effect of endogenously released noradrenaline on prostate smooth-muscle cells resulting in prostate tone reduction and consequently in the improvement of the dynamic aspects of voiding. Several α-blockers are available on the market including alfuzosin, doxazosin, tamsulosin and terazosin which may have different side-effects such as dizziness, hypotension, rhinitis, and abnormal ejaculation. The enzyme 5α-reductase converts testosterone to dihydrotestosterone (DHT), playing a crucial role in the initial development and normal growth of the prostate (114). Finasteride and dutasteride are the two 5-ARIs available on the market. They cause apoptosis of prostatic epithelial cells, resulting in prostate size reduction by an average of 15 - 25% over time (115, 116). The most common adverse events of 5-ARIs are sexual dysfunction including reduced libido and erectile dysfunction (ED) (115).

Purpose of This Study

ANO1 has been suggested to be a regulator of cell proliferation and tumorigenesis, even before it was discovered as a CaCC, and is highly expressed in several carcinomas, including gastrointestinal stromal tumors (94), esophageal squamous cell carcinoma (117), head and neck squamous cell carcinoma (91), oral cancer cells (93), breast cancer (118), and prostate cancer (119). The disruption of Ano1 or the administration of a pharmacological ANO1 inhibitor impairs the proliferation of interstitial cells of Cajal (62, 120) and numerous cancer cells (118, 119, 121). ANO1 promotes tumorigenesis and cancer progression by inducing epidermal growth factor receptor-activated mitogen-activated kinase (MAPK)/AKT signaling (118) and regulates tumor cell motility and metastasis via the ezrin/radixin/moesin protein family (122). Thus, ANO1 is considered to be a potential target for anticancer therapy (123).

The availability of testosterone or DHT is known to cause the development of histologically characterized BPH (101). Clinical reports on BPH have suggested a positive association between BPH and prostate

cancer, with increased risk of and mortality from prostate cancer among BPH patients (124). However, some epidemiologic studies have reported that BPH is not a cause of prostate cancer (125, 126). Despite the controversy on the association between prostate cancer and BPH, common risk factors for the two diseases include chronic inflammation, metabolic disturbance, and genetic variation (127). Regardless of its association with prostate cancer, BPH is still a social issue for the elderly, but the etiologic mechanisms of its pathology remain unknown.

Thus, this study was performed to determine whether ANO1 plays a key role in testosterone-dependent prostate hyperplasia by exploring the pathophysiological roles of ANO1 in hyperplasia and identifying a molecular signaling related ANO1 downstream pathway.

Methods

1. Cell culture and transfection

RWPE-1 cells (normal human prostate epithelial cells) and PC3, LnCap cells (human prostate carcinoma cells) were purchased from ATCC and cultured in Keratinocyte-SFM (Gibco, USA) and RPMI1640 (Invitrogen, USA) supplemented with 10% fetal bovine serum, respectively. To examine the dose-dependent expression of ANO1 during treatment, DHT (Sigma, A8380) was applied to the cells at a dose of 0.1, 0.3, 1, 3, or 10 μM for 24 h. To quantify the time-dependent expression of ANO1, the cells were treated for 1, 2, 4, or 8 h with 2 μM DHT. For live cell imaging, cells transfected with either scrambled or Ano1 siRNA using Lipofectamine 2000^{TM} were plated onto a 24-well plate and incubated with 10 nM DHT in a humidified live cell imaging chamber with 5% CO_2, 90% N_2, and 5% O_2. The plates were photographed every hour for 120 h with an IncuCyte ZOOM automated microscope system (Essen BioScience, USA). For the knockdown experiment, we used siRNA for ANO1 targeting human Ano1 (5'- GUCCAACAUCCGGGUCACA-3') and scrambled siRNA (5'-ACGAAAUUGGUGGCGUAGG-3'). For AR knockdown, two types of

siRNA were used: target sequence of AR siRNA1 (5'-UGGGUGUCACUAUGGAGCU-3') and AR siRNA2 (5'-CUGAUCUGGUUUUCAAUGA-3') targeting against human AR. siRNAs were obtained from BIONEER (Korea).

2. Human specimens

The human BPH tissue microarray slide was purchased from Biomax Inc. (US, PR804). BPH pathologic tissues were obtained from the Samsung Medical Center (Korea).

3. Western blot

To lyse the cells, M-PER (Mammalian Protein Extraction Reagent; Thermo, USA) and a complete protease and phosphatase inhibitor cocktail (Roche, USA) were added to the culture dishes. RWPE-1 cells were then scraped off and moved to centrifuge tubes. The supernatant whole cell extracts were obtained, and the BCA™ Protein Assay Kit (Pierce, USA) was used to determine the protein concentrations. The proteins were then denatured at 100℃ and separated on a 4-12% NuPAGE® Bis-Tris gel (Invitrogen, USA) and transferred onto nitrocellulose membranes. After

blocking with 5% skimmed milk, the membranes were incubated with anti-ANO1 (1:1000, Abcam, ab53212), phospho-PTEN (1:2000, Cell signaling, #9551), pan-AKT (1:2000, Cell signaling, #4691), phospho-AKT(Ser473) (1:2000, Cell signaling, #4060), Erk1/2 (1:2000, Cell signaling, #9102), phospho-Erk1/2(Thr202/Tyr204) (1:2000, Cell signaling, #9101), or PCNA (1:2000, Santa Cruz, FL-261) antibodies and anti-rabbit immunoglobulin (Ig) G-horseradish peroxidase (HRP) secondary antibody (1:2000, Cell signaling, 7074S) overnight at 4°C, and β-actin (1:5000, Sigma, A2066) was used for normalization. The bands were visualized using the ECL reagent (Pierce, USA) and quantified using ImageJ software (http://imagej.nih.gov/ij/).

4. Patch clamp recording

RWPE-1 cells were plated onto poly-L-lysine-coated glass coverslips and pretreated with DHT for 18-24 h. Whole cell patch clamp recording was performed at a holding potential of –60 mV at room temperature. Patch electrodes were filled with a solution containing 140 mM NMDG-Cl^-, 2 mM $MgCl_2$, 5 mM EGTA, 10 mM HEPES, and 1 mM ATP (pH 7.4) plus $CaCl_2$ to obtain the desired free Ca^{2+} concentration (10 μM). The bath solution contained 140 mM NMDG-Cl^-, 2 mM $MgCl_2$, 5 mM EGTA, and 10 mM HEPES, pH 7.2. The step voltages were applied from –100 to +100

mV in 20-mV increments starting from a holding potential of –60 mV. Tannic acid (TA, Sigma, 403040), niflumic acid (NA, Sigma, N0630), 5-nitro-2-(3-phenylpropylamino) benzoic acid (NPPB, Sigma, N4779), MONNA (Sigma, SML0902), CACCinh-A01 (Sigma, SML0916), and T16Ainh-A01 (Sigma, SML0493) were diluted in bath solution. Recordings were performed with an Axopatch 200B amplifier and digitized using Digidata 1440 (Molecular Devices). The data were analyzed by pClamp software (version 6.0, Molecular Device).

5. Immunofluorescence

RWPE-1 cells were seeded on poly-L-lysine-coated coverslips in an eight-well plate for 24 h prior to treatment and were then treated for 48 h with DHT. Treated cells were fixed in 4% paraformaldehyde and permeabilized with 0.2% Triton X-100 in phosphate buffer solution (PBS). After a 30-min blockage with blocking solution (5% bovine serum albumin (BSA) in PBS), the cells were incubated with anti-ANO1 (1:1000, Abcam, ab53212) antibody overnight at 4℃, then washed with PBS and incubated with a secondary antibody conjugated with Alexa Fluor® 546Dye (1:400, Invitrogen) for 1 h. Nuclei were stained by Hoechst for 5 min. After washing three times with PBS, the coverslips were mounted with

Vectashield® (Vector Laboratories, USA) and images were captured using a Zeiss LSM 700 Confocal (Carl Zeiss).

6. Reporter gene assay

For the luciferase reporter encoding FR1, FR2, FR3, and FR4, the region of the mouse Ano1 promoter from -3000 to +78 relative to the transcription start site, was amplified by polymerase chain reaction (PCR) and cloned into the pGL3 basic vector. The MMTV-luciferase reporter plasmid (MMTV-luc) containing four inverted repeats of the 5'-TGTTCT-3' sequence was used as a positive control. All of the new constructs were verified by DNA sequencing. The measurement of the transient expression of proteins and reporter gene analysis in RWPE-1 cells were performed using FuGENE HD Transfection Reagent (Roche, Indianapolis, IN) according to the manufacturer's instructions. The CMV-β-gal vector was co-transfected for transfection efficiency in each sample. The cells were treated with 1 or 10 nM DHT or vehicle for 24 h, then harvested and lysed. The luciferase activity was determined as fold activation compared with the vehicle-treated group which was normalized to β-gal activity for each sample using the Luciferase assay system according to the manufacturer's instructions (Promega, Madison, WI).

7. Chromatin immunoprecipitation assay

To analyze the binding of AR to the potential AR binding region of the Ano1 promoter, chromatin immunoprecipitation assay was performed using the SimpleChIP enzymatic chromatin IP kit (Cell Signaling Technology, Danvers, MA) according to the protocol provided by the manufacturer. Briefly, the chromatin, cross-linked to proteins, was digested with micrococcal nuclease. The digested chromatin was immunoprecipitated with control IgG or anti-AR (Millipore, Billerica, MA, USA) antibodies. The DNA-protein cross-links of immunoprecipitants were reversed and then the DNA was purified. The association between AR and the putative AR binding regions of the ANO1 promoter was analyzed by PCR using the following primer sets: 5'-CGG AGC TTC CCA TAA TGA AA-3' and 5'-TGC TGG GAT TCT CTC TCC AC-3' for P1 fragment and 5'-CAC ACT CAC GCC CTA CAT CA-3' and 5'-CCT GCT GTC ACT CAG CAC TC-3' for P2 fragment amplification. Each step of the PCR was performed as follows: an initial denaturation step for 5 min at 95 oC; 40 cycles of an amplification step consisting of denaturation for 30 s at 95 oC, annealing for 30 s at 64 oC, and elongation for 30 s at 72 oC, and a final extension step for 7 min at 72 oC. The PCR products were separated by 2% agarose gel

electrophoresis and visualized using a Gel Doc EZ System (Bio-Rad, Hercules, CA)

8. Rat BPH model

Six-week-old male Wistar rats weighing 150–200 g were castrated to exclude the influence of intrinsic testosterone. BPH was generated in rats by subcutaneous injections of 3 mg/kg testosterone propionate (CentrinoLab, UK) for 4 weeks after castration. Castrated rats were divided into four groups (n = 5-8): (i) the castration control group, which received orally administered saline and subcutaneous injections of corn oil; (ii) the BPH-model group, which received orally administered saline and subcutaneous injections of testosterone propionate; (iii) the tannic acid (TA)-treated group, which received TA (150 mg/kg) administered by oral gavage and subcutaneous injections of testosterone propionate; (iv) and the finasteride-treated group, which received finasteride (10 mg/kg), a 5 -reductase inhibitor, as a positive control drug administered orally and subcutaneous injections of testosterone propionate. The drugs were administered orally once daily for 4 weeks. The rats were weighed weekly during the experiments and were killed under anesthesia on day 29; whole prostates were removed, weighed, fixed in paraformaldehyde, and snap frozen.

9. in vivo siRNA rat BPH model

BPH was generated in 6-week-old male Wistar rats by consecutive subcutaneous injections of TP (3 mg/kg) for 14 days after castration. Desalt in vivo purity StealthTM Negative siRNA and Ano1 siRNA (Invitrogen, USA) were orthotopically administered to the prostate by intra-prostatic injection on day 1 and day 8. At day 15, the animals were euthanized and the prostates were weighed. Duplex siRNA sequences against Ano1 are: antisense 5'-CCUGCUCAAGUUUGUGAACUCCUAU-3', sense 5'-AUAGGAGUUCACAAACUUGAGCAGG-3'. Negative control Stealth siRNA having similar GC content as Ano1 siRNA, medium GC (Cat. No.10620-312) was purchased from Invitrogen.

10. Immunohistochemistry and histopathology

The rat prostate specimens were fixed in 10% buffered formalin for 24 h, paraffin-embedded, and cut in 5-μm serial section using a vibratome. After deparaffinization of the sections, endogenous peroxidase activity was quenched with 3% H_2O_2 in methanol for 30 min. Tissue sections were dehydrated through graded alcohols and subjected to antigen retrieval using 10 mM sodium citrate. The sections were blocked with PBS containing 5%

normal goat serum and 0.3% Triton X-100 for 1 h at room temperature and then incubated with anti-ANO1 (1:1000, Abcam, ab53212) antibody or Ki-67 antibody (H-300, Santa Cruz, CA, USA) diluted in PBS containing 1% BSA and 0.3% Triton X-100 overnight at 4℃. They were subsequently washed three times and then incubated for 1 h with HRP-conjugated secondary antibody. After washing, the slides were incubated with 3,3′-diaminobenzidine tetrahydrochloride (DAB, Sigma) and immediately washed under tap water after the color development. All of the slides were stained with H&E. Immunohistochemical and histopathological changes were observed under a light microscope (Carl Zeiss).

11. Statistics

SigmaStat 3.0 software was used for the statistical evaluation. The results are expressed as means ± standard errors of the mean (SEM). One-way analysis of variance followed by the Bonferroni t-test, the Student–Newman–Keuls test, a two-tailed Student t-test, or a chi-squared test was used where appropriate, and significance was determined as $p < 0.05$.

Results

1. DHT increases ANO1 expression in human prostate epithelial cells

The main phenotype of BPH is an increase in cell numbers (101). We therefore determined whether the expression of ANO1 was related to prostate hyperplasia. To induce prostate hyperplasia, we treated normal human prostate epithelial RWPE-1 cells (128) with DHT, an immediate metabolite of testosterone that is metabolized in stromal cells by 5α-reductase and a critical mediator of prostatic growth, and studied the changes in ANO1 expression. Western blot analysis revealed a dose-dependent increase in ANO1 expression 24 h after DHT treatment (Fig. 1A). The threshold concentration was 1 μM. ANO1 expression was detected as early as 1 h after incubation with 2 μM DHT (Fig. 1B). ANO1 immunoreactivity in RWPE-1 cells increased in a dose-dependent manner after the treatment with DHT, whereas only weak ANO1 immunoreactivity was observed in vehicle-treated RWPE-1 cells (Fig. 2). Following treatment with 10 μM DHT, 89% of cells were ANO1-positive. These results indicate that ANO1 is upregulated by DHT in prostate epithelial cells (Fig. 3).

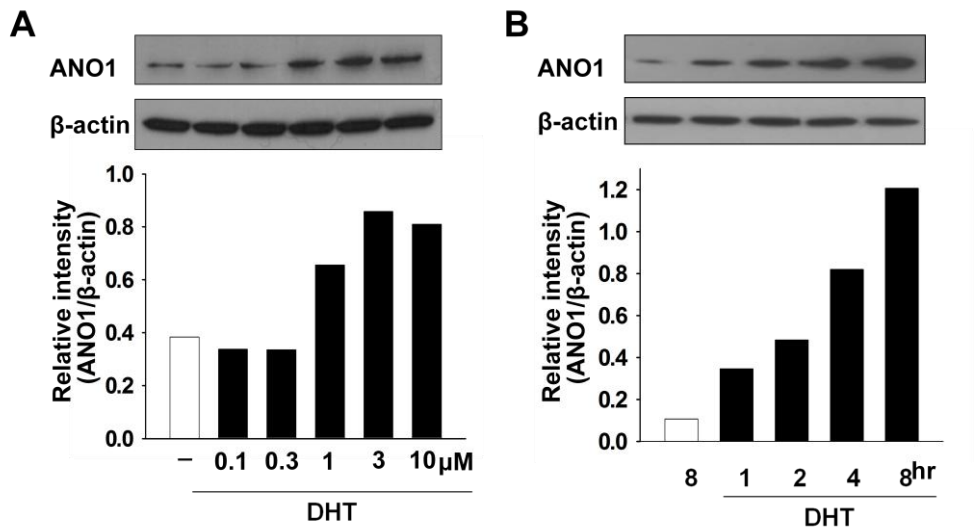

Figure 1. Dose- and Time-dependent increase of ANO1 in RWPE-1 cells

Dihydrotestosterone (DHT) increases ANO1 expression and the proliferation of human prostate epithelial cells. (A, B) Western blot analysis of ANO1 in the RWPE-1 cells cultured with DHT in a dose- (0.1, 0.3, 1, 3, 10 μM for 24h) and time- (1, 2, 4, 8h at 2 μM) dependent manner. The lower panels show a quantification of band intensities analyzed by ImageJ software. The ANO1 band intensity was normalized to β-actin.

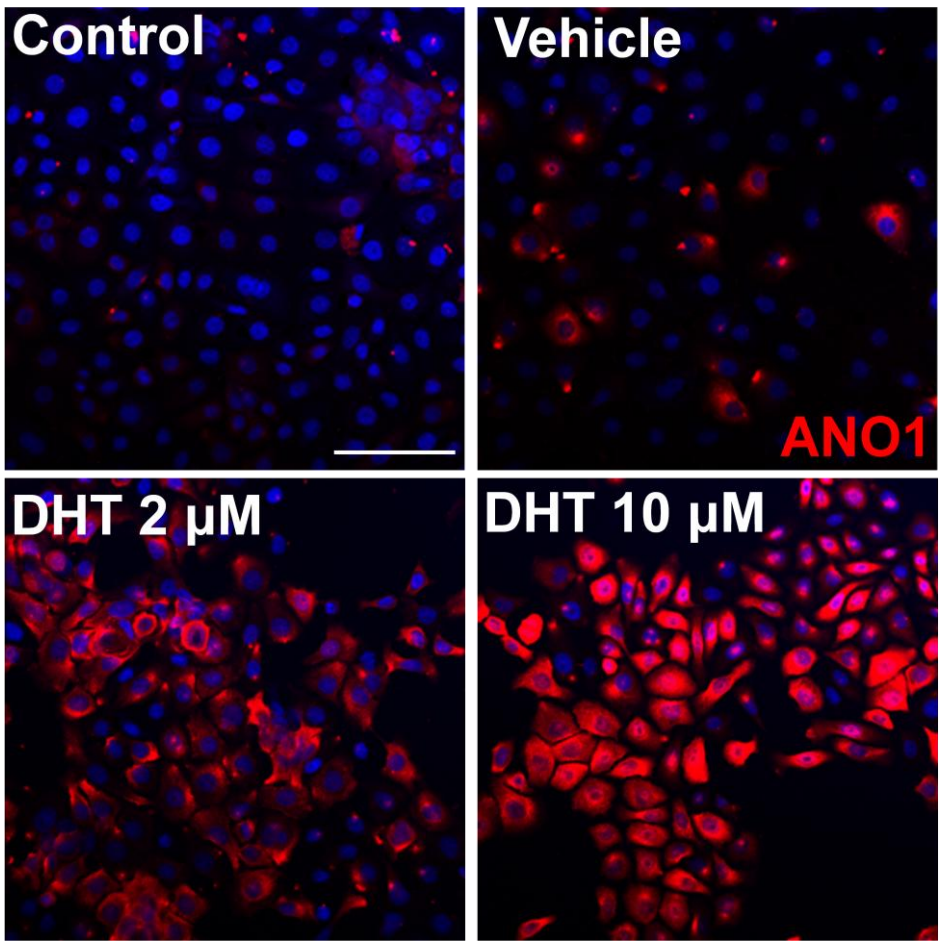

Figure 2. Immunofluorescence analysis of ANO1 in RWPE-1 cells

Representative confocal microscopy images stained with ANO1 (red) and Hoechst (blue) in vehicle- or DHT-treated RWPE-1 cells for 48 h. The scale bar represents 50 μm.

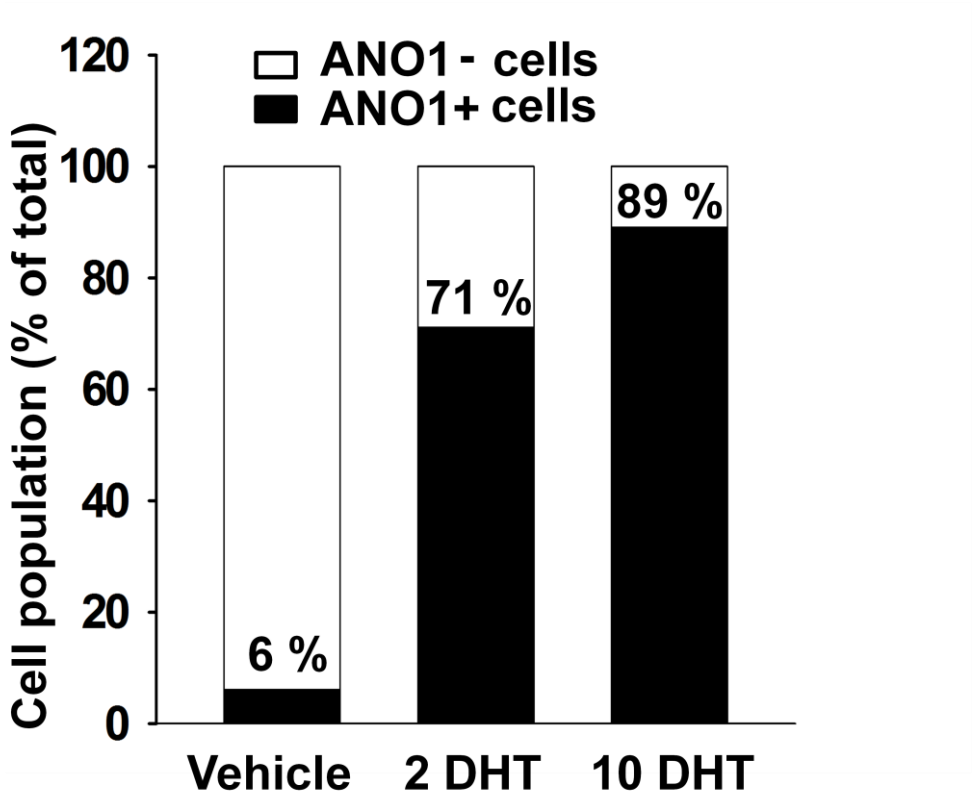

Figure 3. Immunofluorescence analysis of ANO1 in RWPE-1 cells

Immunofluorescence quantification of ANO1-positive and -negative cells. Ten slides were counted for every group (1,067 cells for vehicle; 549 cells for 2 μM DHT; 510 cells for 10 μM DHT).

2. Activation of the ANO1 promoter-driven luciferase reporter gene in RWPE-1 cell

Because of the increase in ANO1 expression after DHT treatment, it was conceivable that DHT controls the transcription of Ano1. Using the MatInspector search engine program (http://www.genomatix.de), the mouse Ano1 promoter region was searched for the androgen-response element (ARE) that is known to regulate the transcription of androgen-responsive genes (129). After ligand binding, androgen receptors (ARs) are known to recognize and bind the ARE region leading to subsequent transcription (130). When the -3,000-bp promoter region upstream of the transcriptional initiation site of Ano1 was analyzed, three ARE consensus sites were found. As shown in Fig. 2A, the three putative AREs (ARE1, ARE2, and ARE3) were located at -997 ~ -979, -891 ~ -873, and -206 ~ -188 bp upstream of the start codon, respectively. We then performed a luciferase reporter assay to determine whether testosterone acted on the AREs to stimulate the transcription of Ano1. The promoter–luciferase constructs FR1, FR2, FR3, and FR4 were created, containing, respectively, ARE1 + ARE2 + ARE3, ARE2 + ARE3, ARE3 alone, and none of the three (Fig. 4). The mouse mammary tumor virus promoter (MMTV)–luciferase reporter plasmid (MMTV-luc) containing four inverted repeats of the 5’-TGTTCT-3’ sequence was used as a positive control (130). The promoter activities of

these constructs were examined in RWPE-1 cells which, after transfection of the reporter plasmid, were treated with DHT for 24 h and lysed for luciferase activity. A 5~6-fold increase in luciferase activity was observed in cells transfected with the FR1 and FR2 constructs in a dose–dependent manner (Fig. 5). A smaller increase was found in FR3-transfected cells, but no increase occurred in cells transfected with the blank (FR4) constructs. Simultaneously, the level of the Ano1 transcript was increased in RWPE-1 cells after treatment with DHT, but was blocked after transfection with small interfering RNAs (siRNAs) of the AR (Fig. 6).

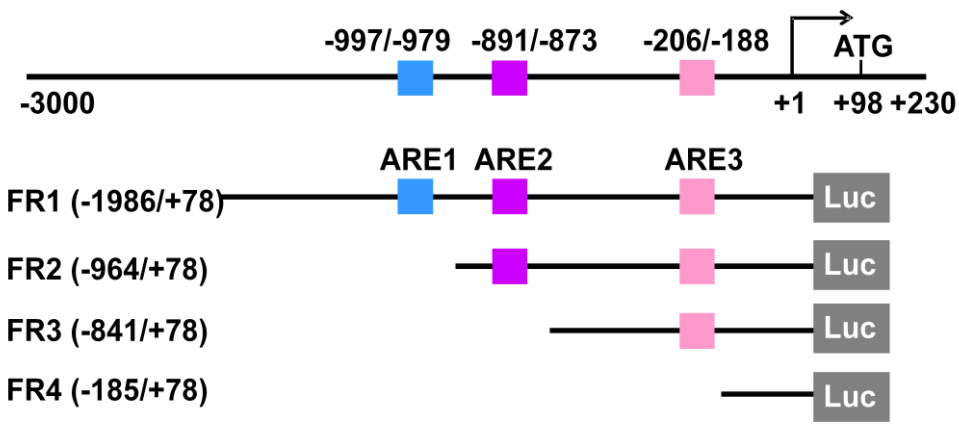

Figure 4. Schema of ANO1 promoter-luciferase constructs

Schema of ANO1 promoter-luciferase (Luc) constructs used for reporter gene assays.

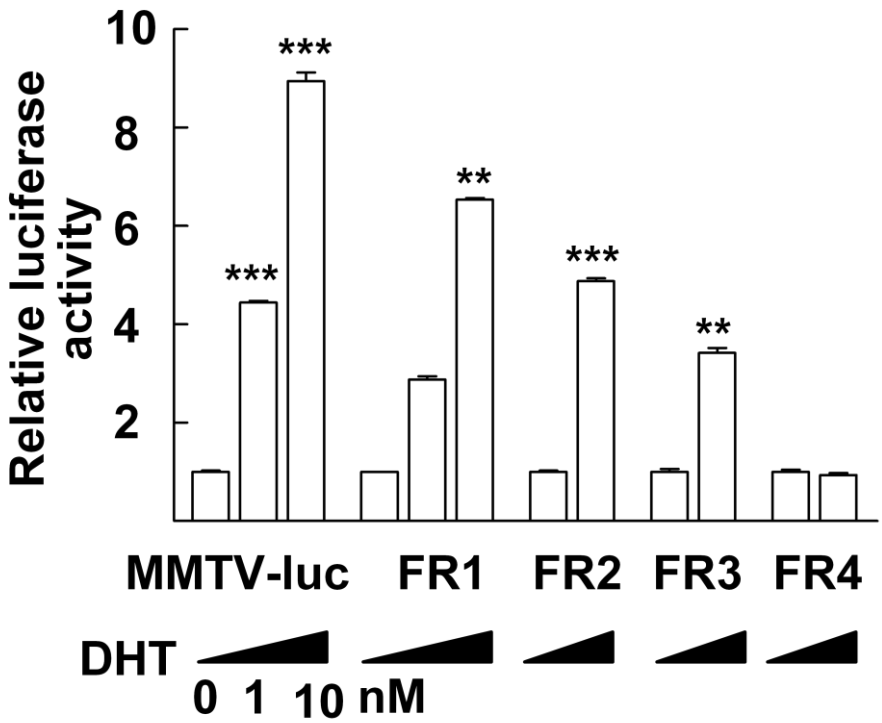
Relative luciferase activity
10
8
6
4
2
***
***
**
***
**
MMTV-luc
FR1
FR2
FR3
FR4
DHT
0 1 10 nM

Figure 5. Luciferase reporter assay in RWPE-1 cells

The luciferase reporter assay shows that three ARE elements are necessary for DHT-induced promoter activation. The RWPE-1 cells were transiently transfected with mouse ANO1 promoter FR1, FR2, FR3, and FR4-Luc or MMTV-Luc and with CMV-β-gal as an internal control. After 4 h of transfection, the cells were treated with 1 or 10 nM DHT or vehicle, as indicated, for 24 h. Cells were harvested and luciferase activity was determined as the luciferase activity normalized to β-gal activity for each sample. Normalized luciferase activity is presented as fold activation. One result representative of at least three independent experiments with similar results is shown. **$p < 0.01$, and ***$p < 0.001$ compared with the vehicle-treated control (One-way ANOVA).

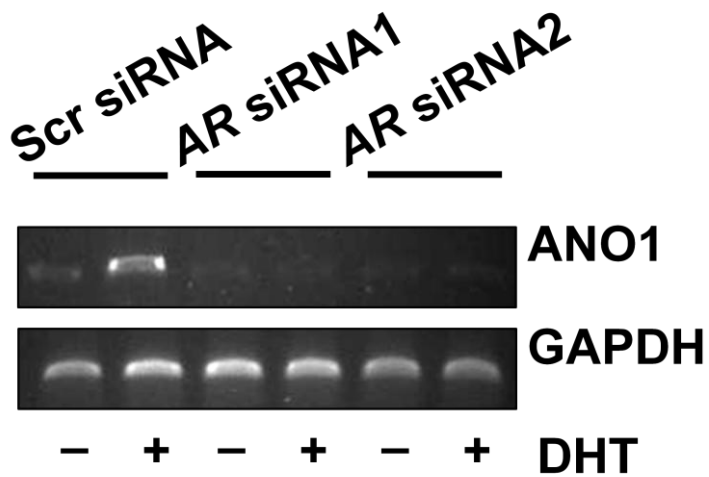

Figure 6. RT-PCR analysis of ANO1 in RWPE-1 cells

The RWPE-1 cells were transfected with scrambled siRNA or AR siRNAs for 48 h and then treated with 10 nM DHT or vehicle for 24 h. mRNA levels were measured by reverse transcriptase-PCR.

3. A ChIP assay for the AR binding to the ANO1 promoter in RWPE-1 cells

We next performed a chromatin immunoprecipitation (ChIP) assay to verify in vivo interaction of the AR with the ANO1 promoter region. To do this, the human promoter region of Ano1 was searched for the putative ARE regions. There were two putative ARE regions found in the human promoter region (Fig. 7). The chromatin fragments from RWPE-1 cells cultured in presence of vehicle or 10 nM DHT were immunoprecipitated with anti-AR antibody or control rabbit IgG. Then, around 200 bp fragments of ANO1 promoter (designated as P1 and P2) were amplified by PCR using two sets of primers directed to cover the two putative ARE sites. In agreement with the results from the reporter gene assay (Fig. 5), the binding of AR to the two putative AR-binding sites was clearly increased in RWPE-1 cells treated with DHT for 24 h (Fig. 8). These results further confirm that testosterone can activate the Ano1 promoter through direct interaction of AR and ARE in the ANO1 promoter.

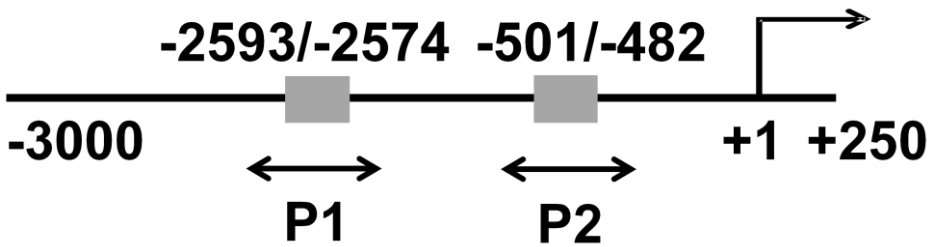

Figure 7. Schematic representation of hAno1 promoter fragment

Schematic representation of hAno1 promoter fragment. Putative ARE sites are illustrated (grey box).

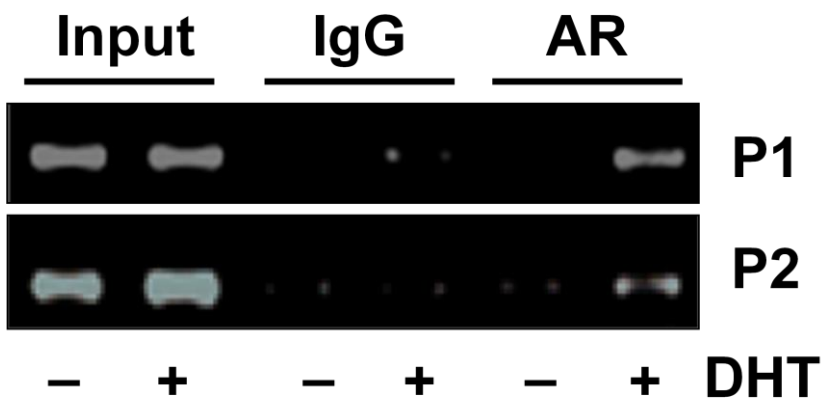

Figure 8. ChIP assay for the AR binding to the ANO1 promoter in RWPE-1 cells

The chromatin was cross-linked to proteins, digested with micrococcal nuclease, and immunoprecipitated with control IgG (IgG) or anti-AR (AR) antibodies. The DNA-protein cross-links of the immunoprecipitants were reversed. DNA was purified and the regions (P1 and P2) containing the each ARE site was amplified with two probes. RWPE-1 cells were treated with vehicle or 10 nM DHT for 24 h. An equal amount of input chromatin (Input) was applied.

4. Ano1 knockdown abolishes DHT-induced prostate cancer cell proliferation

Because DHT upregulates ANO1, it is conceivable that ANO1 expression contributes to the hyperplasia. To address this issue, we examined whether the knockdown of Ano1 affects cell proliferation. Because RWPE-1 cells have a low level of endogenous ANO1, human prostate cancer PC3 and LnCap cells, which have a high basal level of endogenous ANO1, were used to determine the effect of Ano1 knockdown (119). Western blot analysis showed that PC3 and LnCap cells expressed ANO1 at the basal level and the transfection of Ano1 siRNA effectively silenced the endogenous expression of ANO1 in both cells (Fig. 9A and B). DHT (100 nM) treatment induced the proliferation of PC3 and LnCap cells transfected with scrambled siRNA whereas it failed to induce the proliferation of PC3 and LnCap cells transfected with Ano1 siRNA (Fig. 10 and 11).

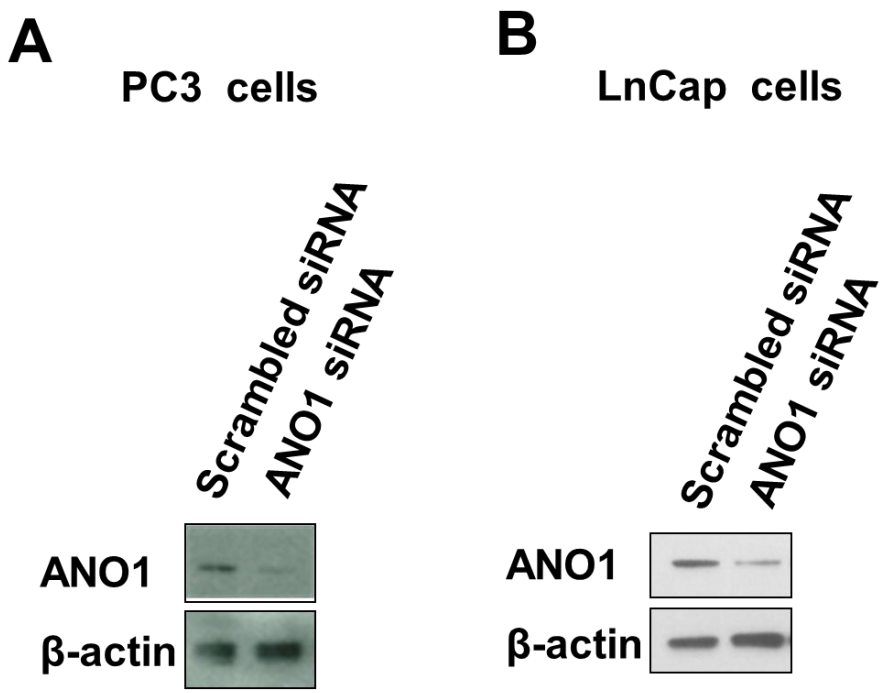

Figure 9. ANO1 knock down by siRNA in PC-3 and LnCap cells

(A) Western blot analysis of ANO1 in PC3 cells transfected with scrambled (Scr) siRNA or Ano1 siRNA.

(B) Western blot analysis of ANO1 in LnCap cells transfected with scrambled (Scr) siRNA or Ano1 siRNA.

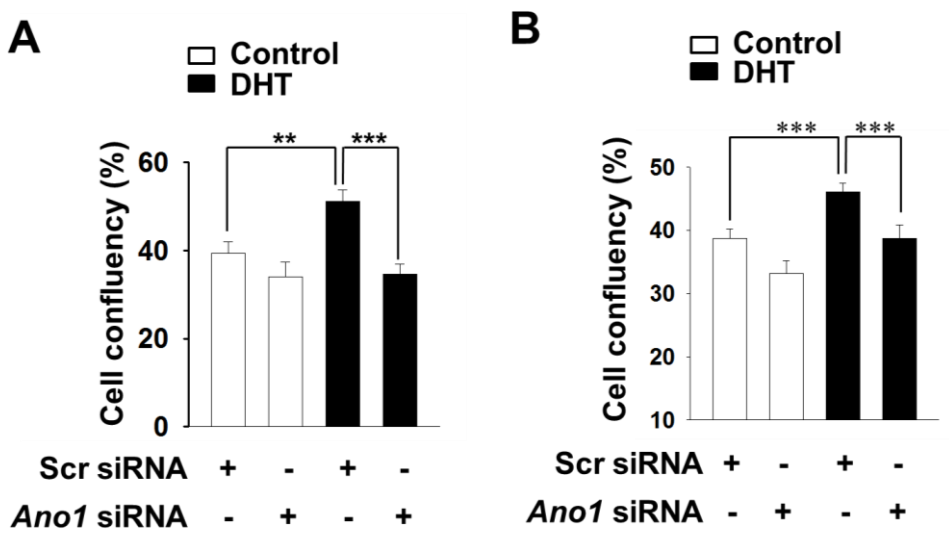

Figure 10. Live cell imaging analysis of DHT induced proliferation

(A) After transfected PC3 cells were incubated with 100 nM DHT for 3 days, the cells were photographed every hour for 120 hrs with an IncuCyte ZOOM automated microscope system. Confluency was calculated by measuring the fraction area occupied by cells of each well.

(B) Effect of Ano1 knock-down on DHT induced cell proliferation in LnCap cells.

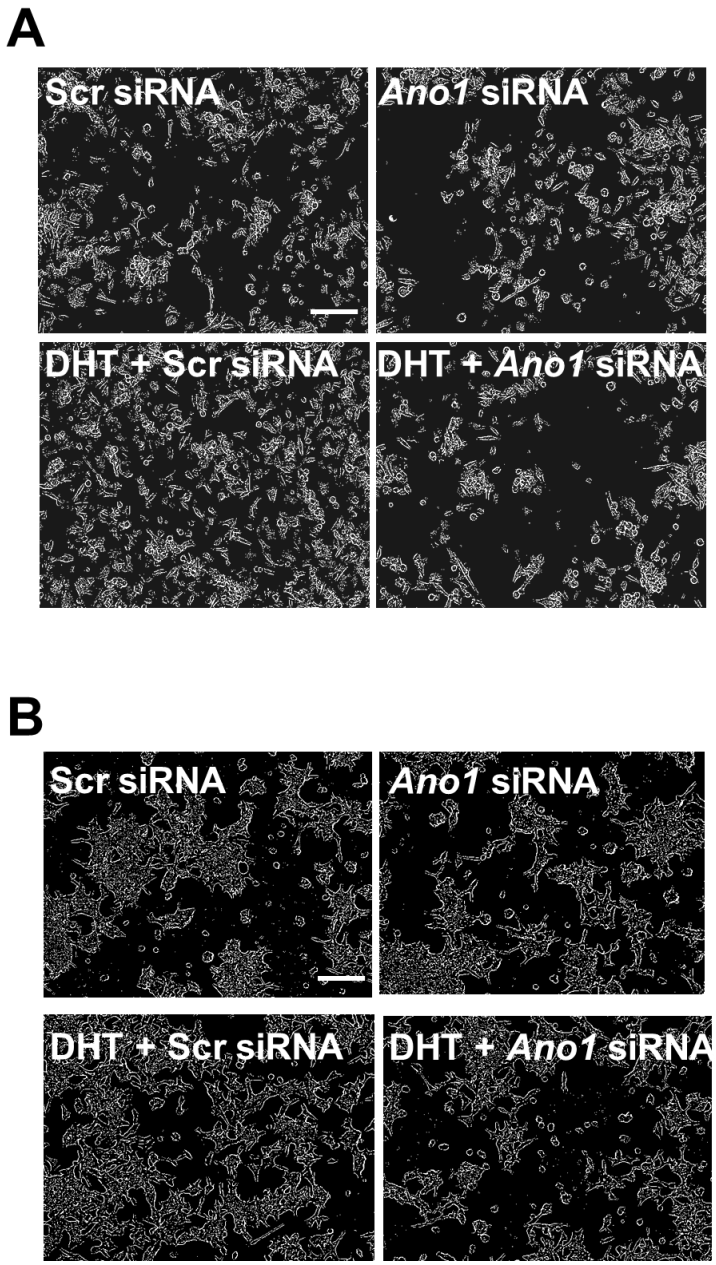

Figure 11. Representative live cell images

Representative live-cell images of PC3 cells (A) and LnCap cells (B).

5. CACC blockers inhibit DHT-induced prostate cancer cell proliferation

Similarly, ANO1 blockers, such as tannic acid, T16inh-A01, CaCCinh-A01, and MONNA, also effectively inhibited the DHT-induced proliferation of LnCap cells (Fig. 12). These results indicate that ANO1 is essential for the DHT-induced proliferation of prostate cells.

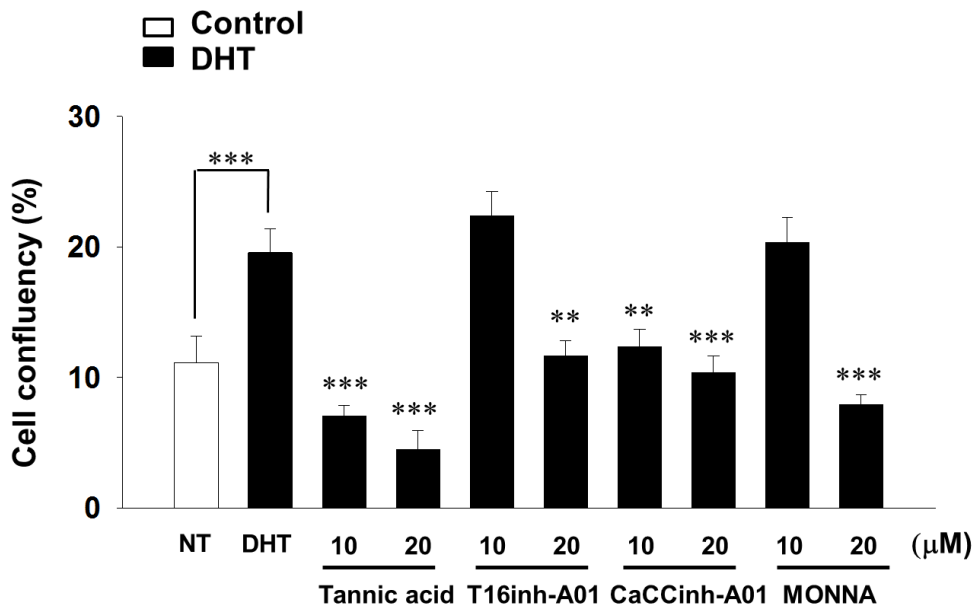

Figure 12. Live cell imaging analysis in CACC blockers treated LnCap cells

Effects of ANO1 blockers, 10 μM or 20 μM tannic acid (TA), T16Ainh-A01, CACCinh-A01, and MONNA on LnCap cell proliferation.

A

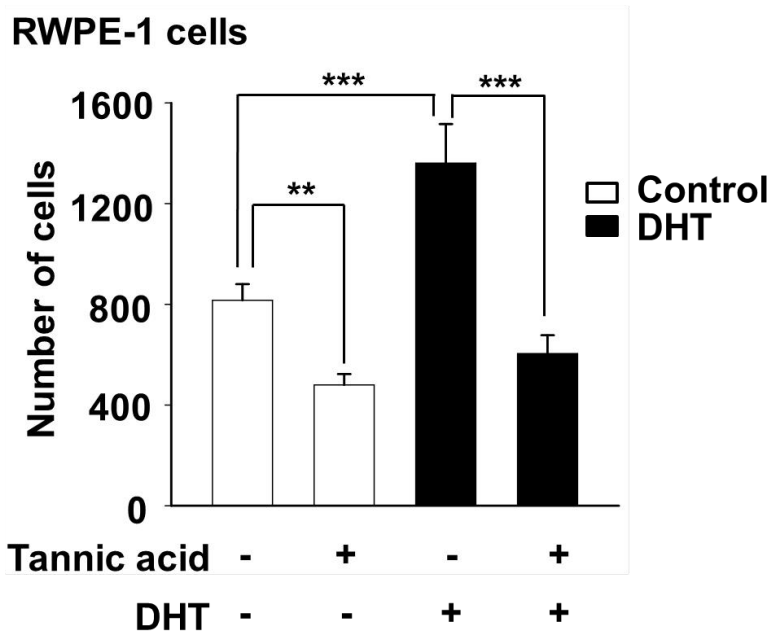
RWPE-1 cells
***
***
**
1600
1200
800
400
0
Number of cells
Control
DHT
Tannic acid - + - +
DHT - - + +

B

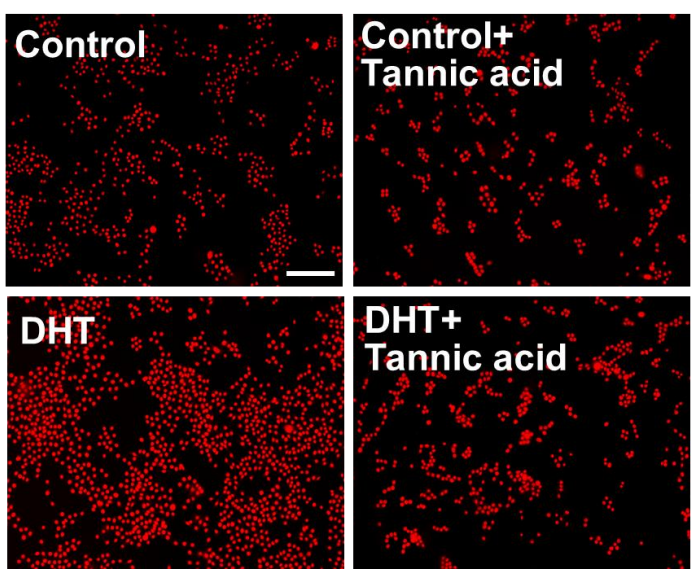
Control
Control+
Tannic acid
DHT
DHT+
Tannic acid

Figure 13. Inhibition of cell proliferation by tannic acid in RWPE-1 cells

(A) RWPE-1 cells were incubated with 10 nM DHT or vehicle for 2 days in the presence or absence of 10 μM tannic acid and the number of cells was counted. Ten slides were counted for every group. **p < 0.01, and ***p < 0.001

(B) Representative fluorescence images. Cells were stained with Hoechest (red). Effects of ANO1 blockers, 10 μM or 20 μM

6. DHT induces ANO1 currents in RWPE-1 cells

We next determined whether DHT upregulates functional ANO1 in RWPE-1 cells by measuring their Ca^{2+}-activated Cl^- currents after treatment with DHT. Cells were voltage clamped to record the whole-cell currents. To obtain Ca^{2+}-activated Cl^- currents, 10 μM Ca^{2+} was added to the pipette solution. Both the pipette and bath solutions contained 140 mM N-methyl-glucamine Cl^- to ensure that Cl^- was the only charge carrier. When a whole-cell was formed at a holding potential of -60 mV, small Cl^- currents with an average amplitude of 91 ± 39 pA (n = 14) were activated in the control cells (Fig. 14 and 15). In contrast, RWPE-1 cells treated with 2 μM DHT for 18-24 h elicited large and robust currents with an amplitude of 575 ± 95 pA (n = 26) (Fig. 14). In addition, the DHT treatment induced an increase in the number of cells responding to the intracellular Ca^{2+} from 14.3% (2/14 cells) to 84.6% (22/26 cells) (Fig. 16).

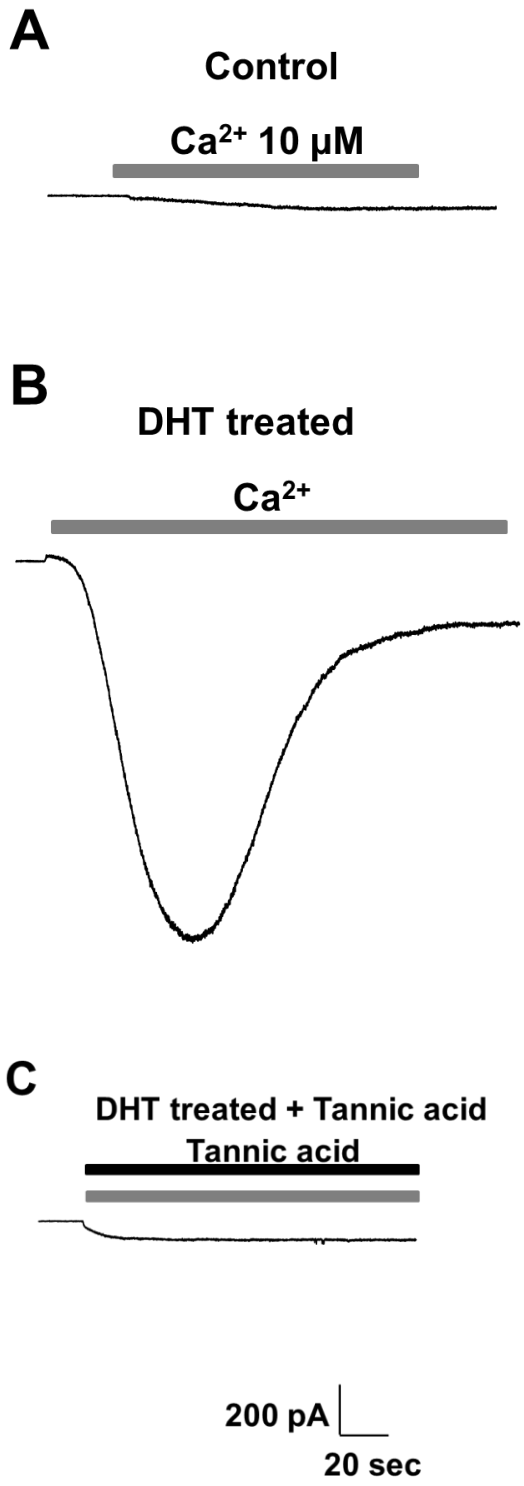
A
Control
Ca2+ 10 µM
B
DHT treated
Ca2+
C
DHT treated + Tannic acid
Tannic acid
200 pA
20 sec

Figure 14. Whole cell currents of DHT treated RWPE-1 cells

Whole cell recording of RWPE-1 cells at a holding potential of -60 mV; 10 μM Ca^{2+}-induced inward current in control (A), DHT-treated (B), and DHT-treated RWPE-1 cells with 10 μM tannic acid (C) when recorded with 10 μM Ca^{2+} in pipette solution. Pipette and bath solutions contained 140 mM NMDG-Cl.

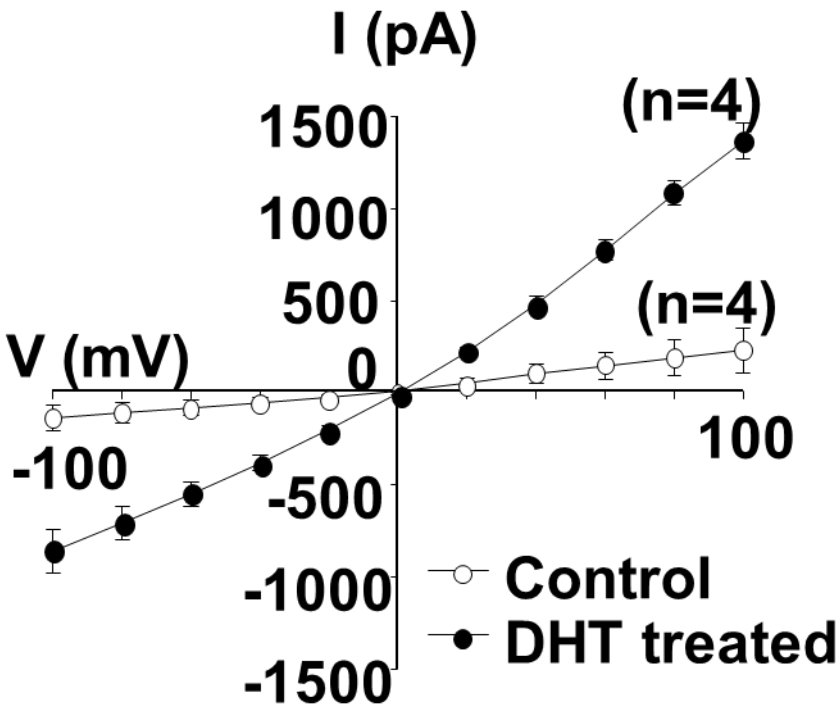

Figure 15. Mean current-voltage (I-V) relationship

Mean current-voltage (I-V) relationship for Ca^{2+}-induced current in control (open circle) or DHT-treated RWPE-1 cells (closed circle).

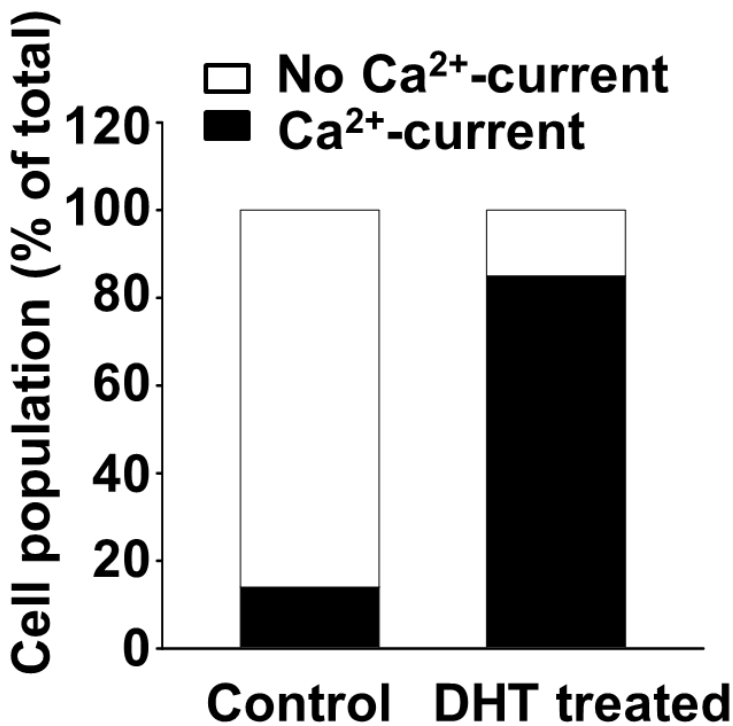

Figure 16. Analysis of cell population in DHT treted RWPE-1 cells

The cell population with Ca^{2+}-induced current out of total cells is shown.

7. CACC blockers inhibit Ca^{2+}-activated ANO1 currents in RWPE-1 cells

These Ca^{2+}-activated currents were inhibited by ANO1 inhibitors, such as tannic acid, niflumic acid, and 5-nitro-2-(3-phenylpropylamino)-benzoate (NPPB), MONNA, CaCCihn-A01, and T16Ainh-A01 (Fig. 17). These results clearly suggest that DHT treatment induces the expression of functional ANO1 in prostate epithelial cells.

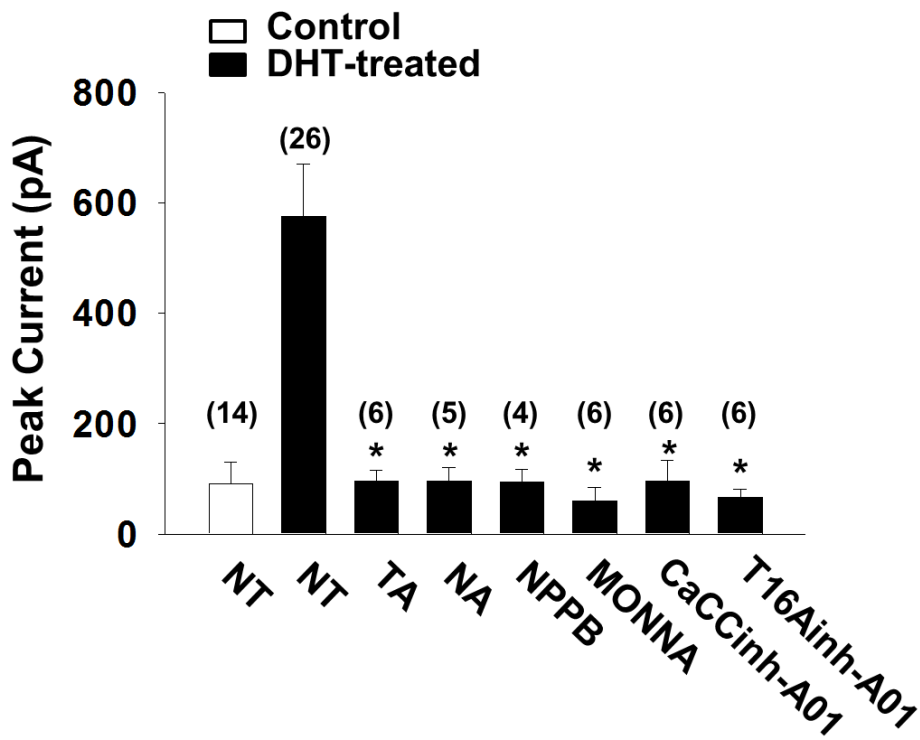

Figure 17. DHT-induced ANO1 currents inhibited by CACC blockers in RWPE-1 cells

Treatment with 10 μM tannic acid (TA), 10 μM niflumic acid (NA), 10 μM 5-nitro-2-(3-phenylpropylamino)-benzoate (NPPB), 5 μM T16Ainh-A01, 20 μM CACCinh-A01, and 10 μM MONNA effectively blocked DHT-induced Ca2+-induced inward current in RWPE-1 cells. NT, not treated. *$p < 0.05$ compared with DHT-treated control cells. Numbers in parenthesis represent experiment numbers.

8. Tannic acid suppresses prostate enlargement in rat BPH model

Next we examined whether the functional inhibition of ANO1 can block testosterone-induced prostate enlargement in vivo. To induce prostate enlargement (a BPH model), 6-week-old male rats were castrated and then treated with testosterone propionate (3 mg/kg, subcutaneous injection) for 4 weeks (Fig. 18). The testosterone-treated group showed a considerable increase in prostate weight compared with vehicle-treated, castrated controls (Fig. 19). As a positive control, a 5α-reductase inhibitor, finasteride, was administered to castrated male rats. Chronic administration of finasteride (10 mg/kg, orally) reduced prostate weight significantly ($p < 0.001$, $n = 8$), suggesting that the development of prostate hyperplasia requires the conversion of testosterone to DHT (Fig. 20). Similarly, when tannic acid (150 mg/kg, orally for 4 weeks) was administered, prostate weight was also significantly reduced ($p < 0.001$, $n = 5$) without body weight loss (Fig. 19 and 20).

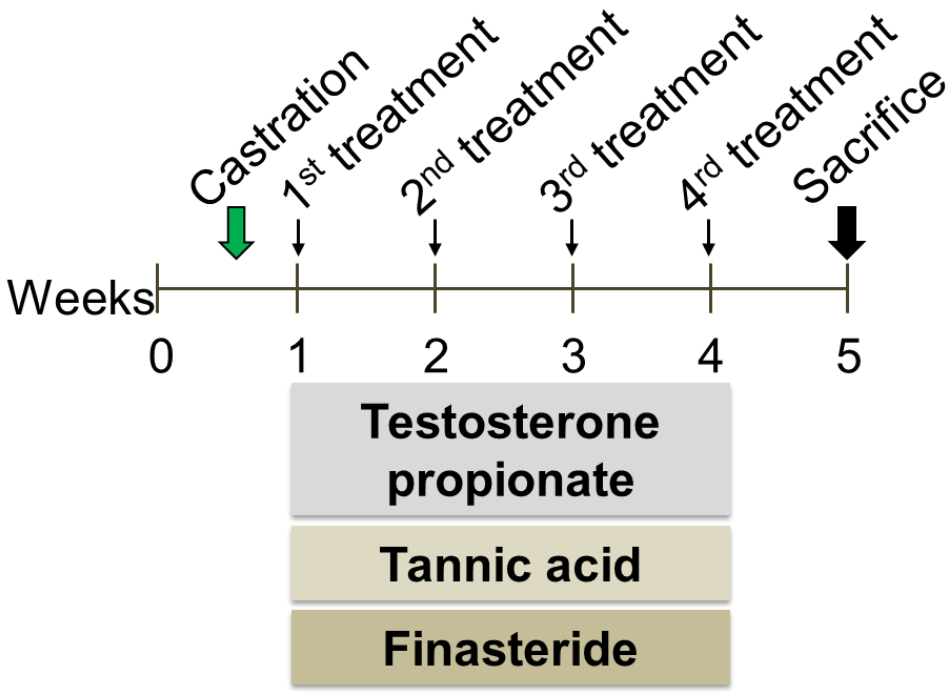

Figure 18. Experimental schema of Rat BPH model

Castration control: subcutaneous injection of corn oil + oral saline; BPH model: subcutaneous injection of 3 mg/kg testosterone propionate + oral saline; Tannic acid: subcutaneous injection of 3 mg/kg testosterone propionate + oral tannic acid (150 mg/kg); Finasteride: subcutaneous injection of 3 mg/kg testosterone propionate + oral finasteride (10 mg/kg).

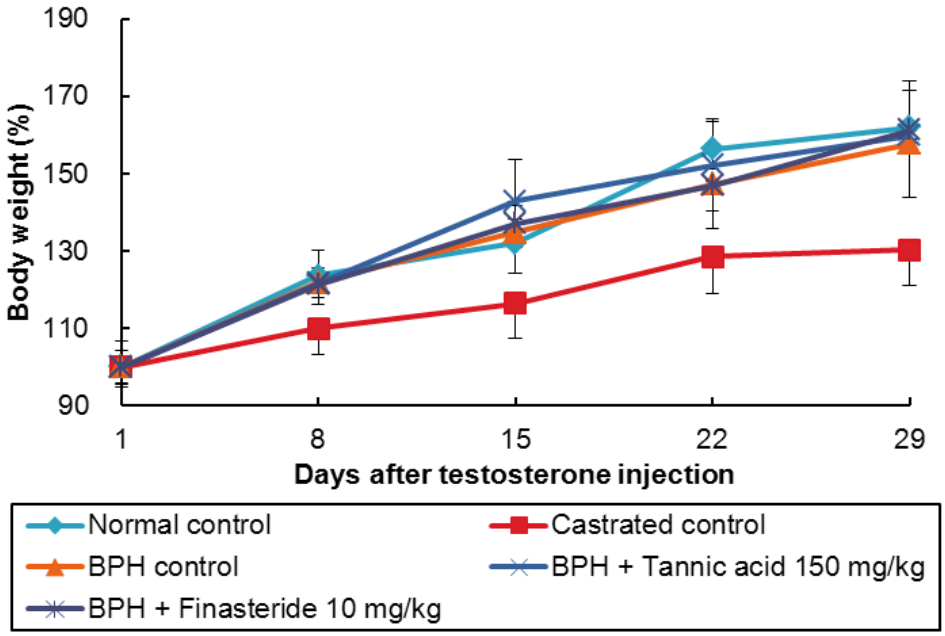

Figure 19. Body weight changes in Rat BPH model

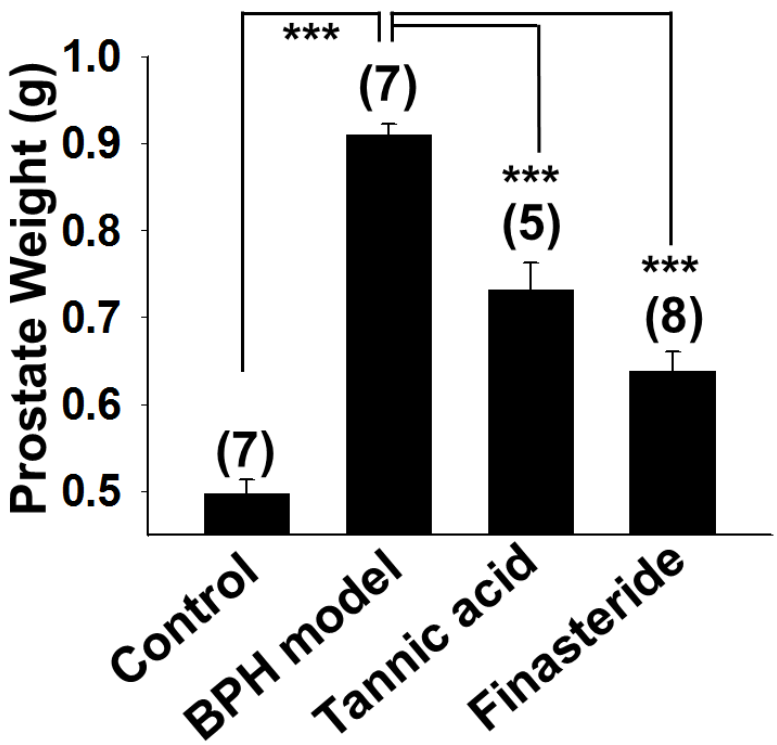

Figure 20. Effects of tannic acid on prostate weight

Effects of tannic acid on prostate weight. ***$p < 0.001$.

9. ANO1 expression increased in prostate tissues from rat BPH model

A post-mortem analysis of ANO1 expression in the BPH-model rats revealed that the levels of both ANO1 messenger RNA (mRNA) and protein were markedly increased (Fig. 21 A and B). A histologic analysis of the prostate further supported the involvement of ANO1 in the hyperplasia. Hematoxylin-eosin (H&E) staining of the prostates from castrated control rats depicted well-arranged monolayers with unfolded acini tapered by low cuboidal epithelial cells and a mild expression of ANO1 (Fig. 22 and 23). In contrast, sections of the prostates isolated from BPH-model rats exhibited thicker epithelial cells with an irregular arrangement and aberrant overexpression of ANO1. Treatment with tannic acid reduced these testosterone-induced abnormalities in rat prostates. These in-vivo results further suggest that ANO1 contributes to testosterone-induced prostate hyperplasia.

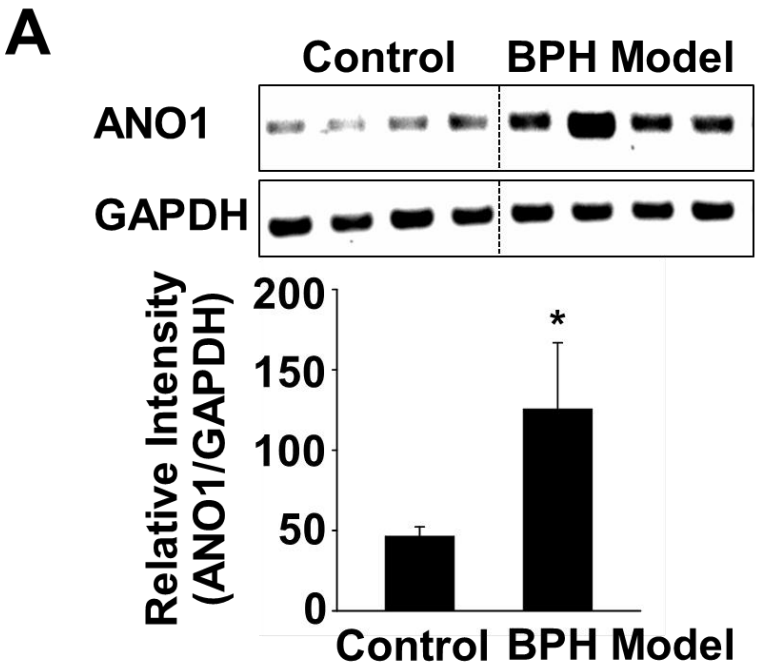
A
Control
BPH Model
ANO1
GAPDH
Relative Intensity
(ANO1/GAPDH)
200
150
100
50
0
*
Control
BPH Model

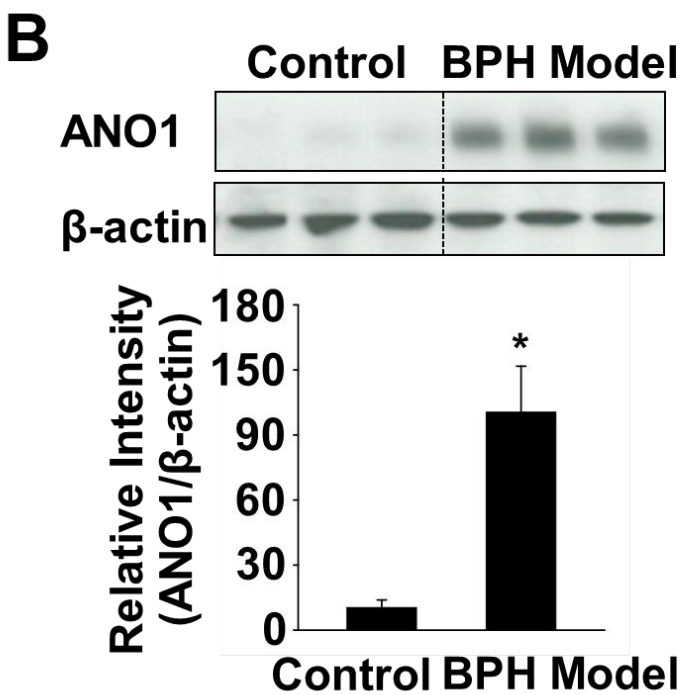
B
Control
BPH Model
ANO1
β-actin
Relative Intensity
(ANO1/β-actin)
180
150
90
60
30
0
*
Control
BPH Model

Figure 21. RT-PCR and Western blot analysis of ANO1 in rat prostate

RT-PCR (A) and Western blot (B) analysis of ANO1 in rat prostate. The band intensities were analyzed by imageJ software. ANO1 band intensity was normalized to GAPDH or β-actin. *$p < 0.01$, compared with castration control.

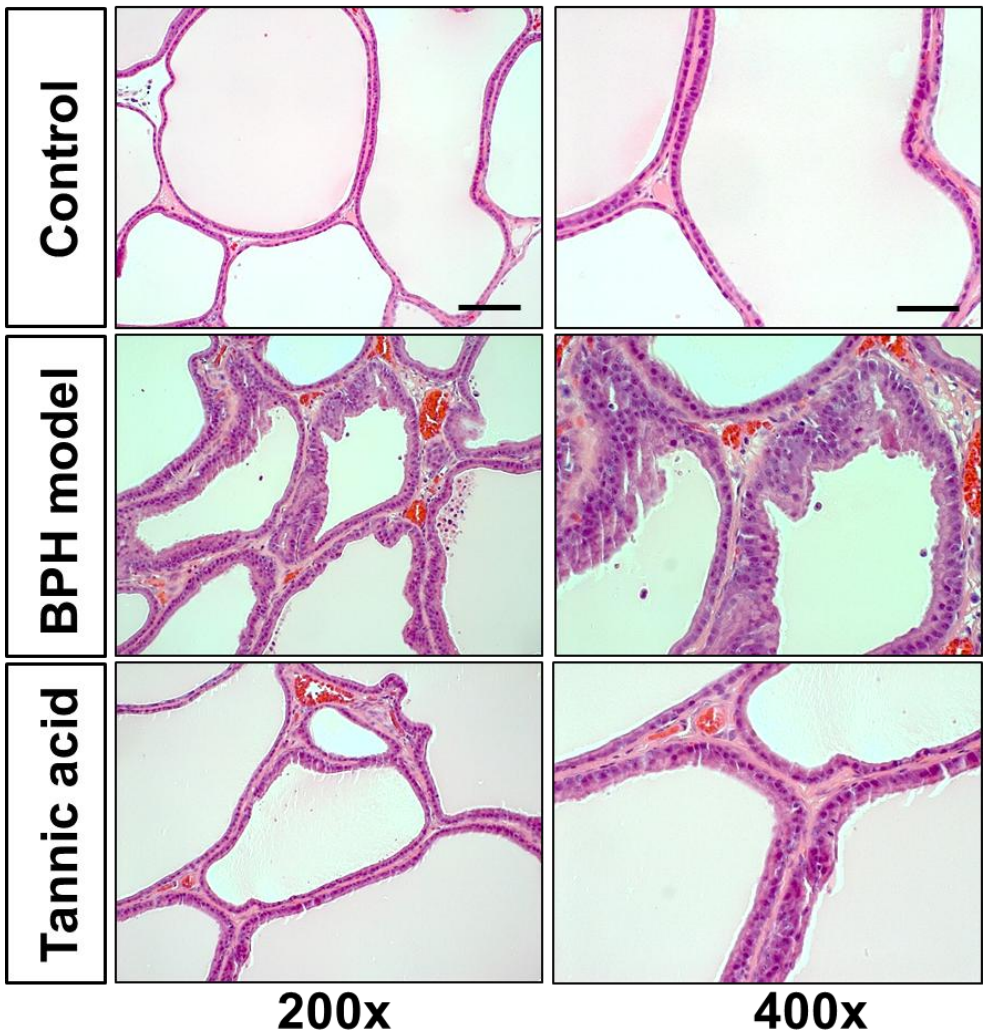

Figure 22. Histological analysis of prostates isolated from Rat BPH model

Paraffin-embedded sections of prostates were stained with H&E. Original magnification, ×200 (left) and ×400 (right); scale bar, 20 μm.

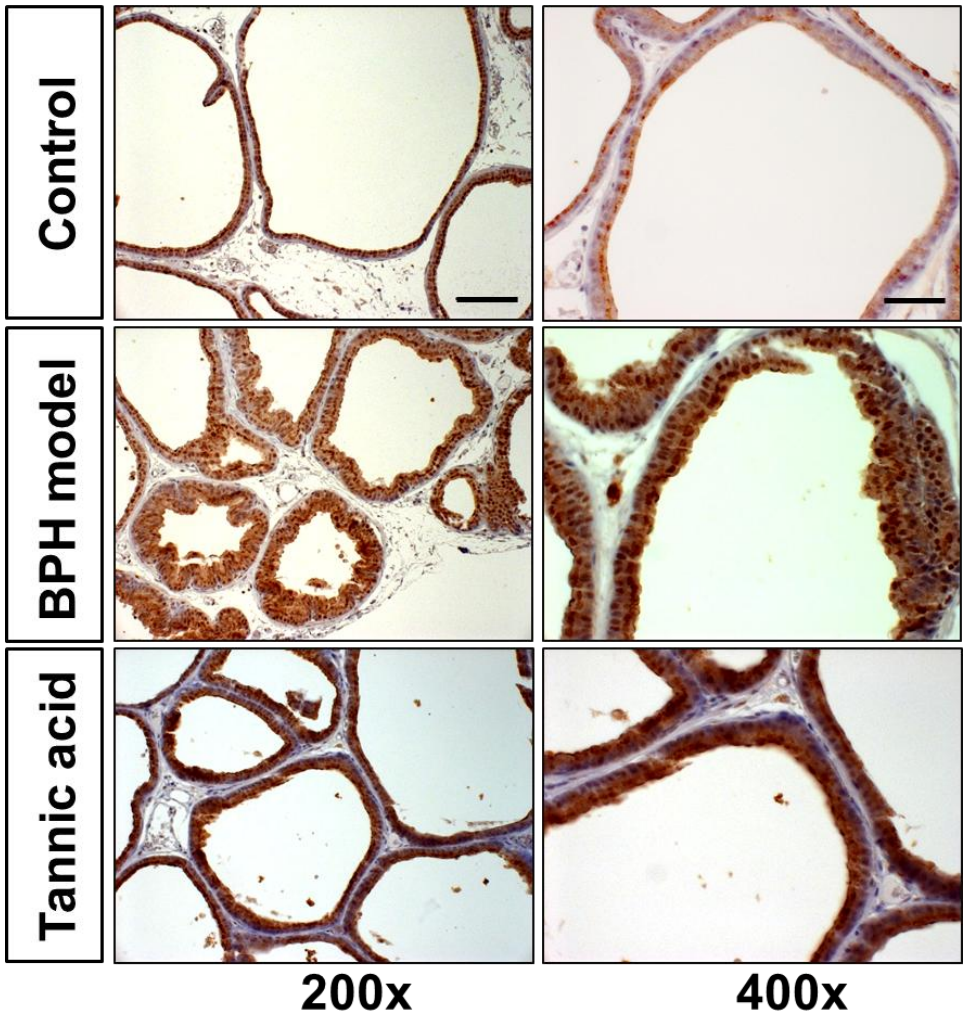

Figure 23. ANO1 immunohistochemistry of prostates isolated from Rat BPH model

Paraffin-embedded sections of prostates were immunostained with ANO1 antibody. Original magnification, ×200 (left) and ×400 (right); scale bar, 20 μm.

10. In-vivo knockdown of Ano1 reduces prostate hyperplasia in rat BPH model

We then induced the in-vivo depletion of Ano1 in the rat prostate by treatment with Ano1 siRNA to investigate whether it can effectively block BPH in vivo. Ano1 siRNA (32-40 μg/rat) was injected directly into the prostate twice (day 1 and 8) after castration of BPH-model rats (Fig. 24). The prostates from testosterone-treated rats showed a marked increase in size and weight relative to castrated controls (Fig. 25 and 26). In contrast, treatment with Ano1 siRNA reduced the prostate weight significantly (60.5 %, $p < 0.001$, $n = 4$-5) whereas prostates injected with scrambled siRNA showed a similar increase in weight to those of BPH-model rats (Fig. 25 and 26). Similarly, intraprostatic injections (day 1, 5, and 9) of ANO1 inhibitors (Fig. 27), T16Ainh-A01, CaCCinh-A01, and MONNA (300 μM in 50 μl/rat), significantly reduced the prostate weights of BPH model rats (Fig. 28 and 29).

We examined whether abnormal histologic changes in the prostates of BPH rats were affected by Ano1 depletion. H&E staining showed highly overgrown epithelial cells in a multi-layer array in the prostates from the BPH-model group compared with those in the control group that had well-arranged epithelial cells in a single layer (Fig. 30). However the histologic

abnormalities were considerably reduced following Ano1 siRNA treatment (Fig. 30). ANO1-immunoreactive cells that were markedly increased along the epithelia in the prostates of BPH-model rats were reduced by treatment with Ano1 siRNA, but not with scrambled siRNA (Fig. 31). These results further suggest that ANO1 plays a key role in testosterone-induced prostate hyperplasia.

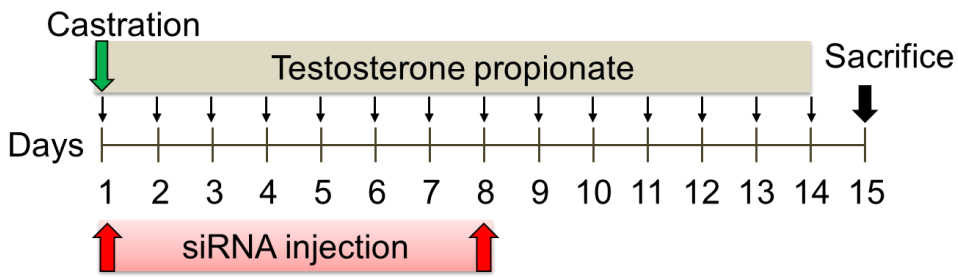

Figure 24. Experimental schema of intraprostatic injection of ANO1 siRNA in Rat BPH model

After castration (day 1), corn oil or 3 mg/kg testosterone propionate was injected subcutaneously for 14 consecutive days. At day 1 and day 8, scrambled siRNA or ANO1 siRNA was injected slowly into the lateral prostate lobes using an insulin syringe.

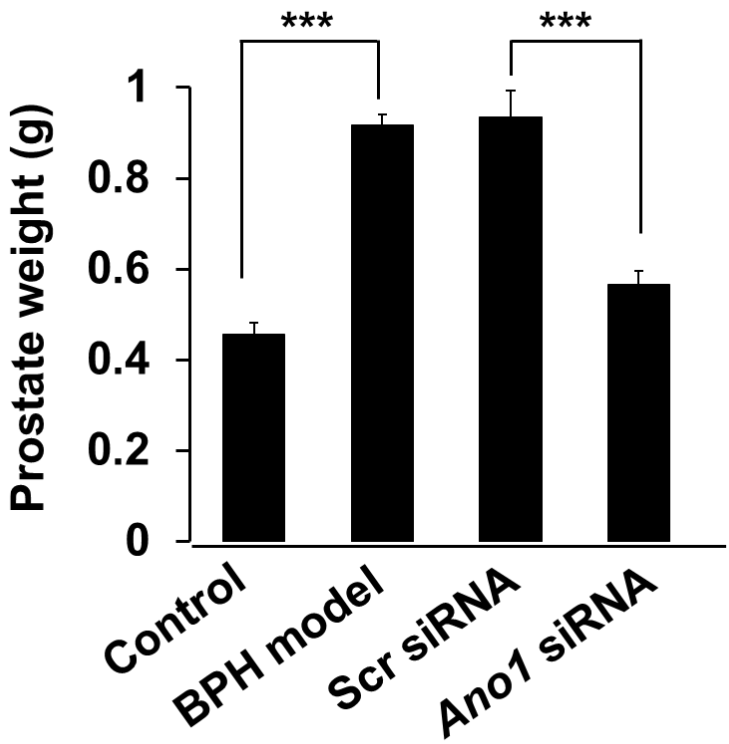

Figure 25. Effects of ANO1 siRNA on prostate weight

Effects of Ano1 siRNA or scrambled siRNA injection on prostate weight. ***$p < 0.001$.

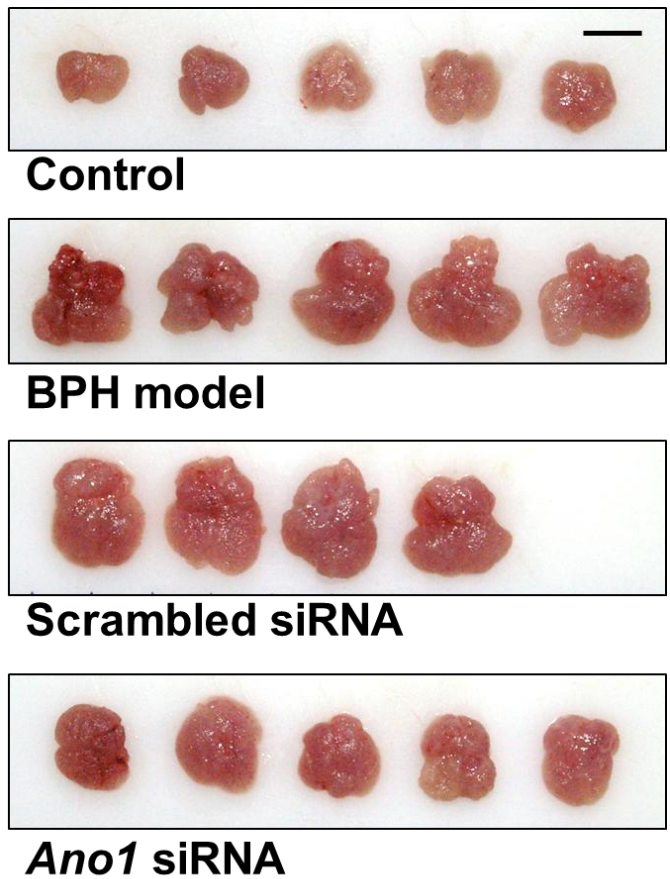

Figure 26. ANO1 siRNA treated prostate photos of Rat BPH model

Comparison of actual prostate size. Scale bar, 1 cm.

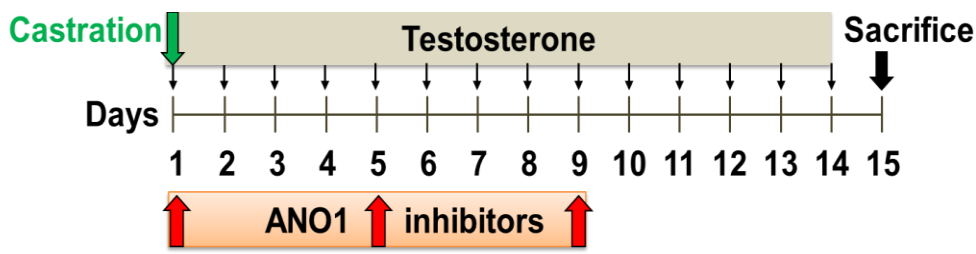

Figure 27. Experimental schema of intraprostatic injection of ANO1 specific inhibitors in Rat BPH model

After castration (day 1), corn oil or 3 mg/kg testosterone propionate was injected subcutaneously for 14 consecutive days. At day 1, 5, and day 9, vehicle saline or ANO1 inhibitors were injected slowly into the lateral prostate lobes using an insulin syringe.

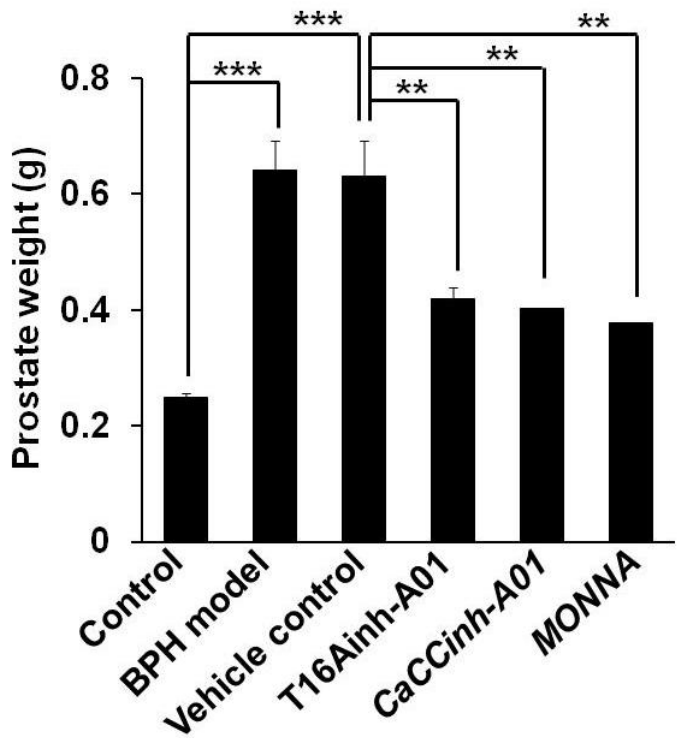

Figure 28. Effects of ANO1 inhibitors on prostate weight

Effects of orthotopic injections of ANO1 antagonists on prostate weight. **, ***$p < 0.01$ and 0.001.

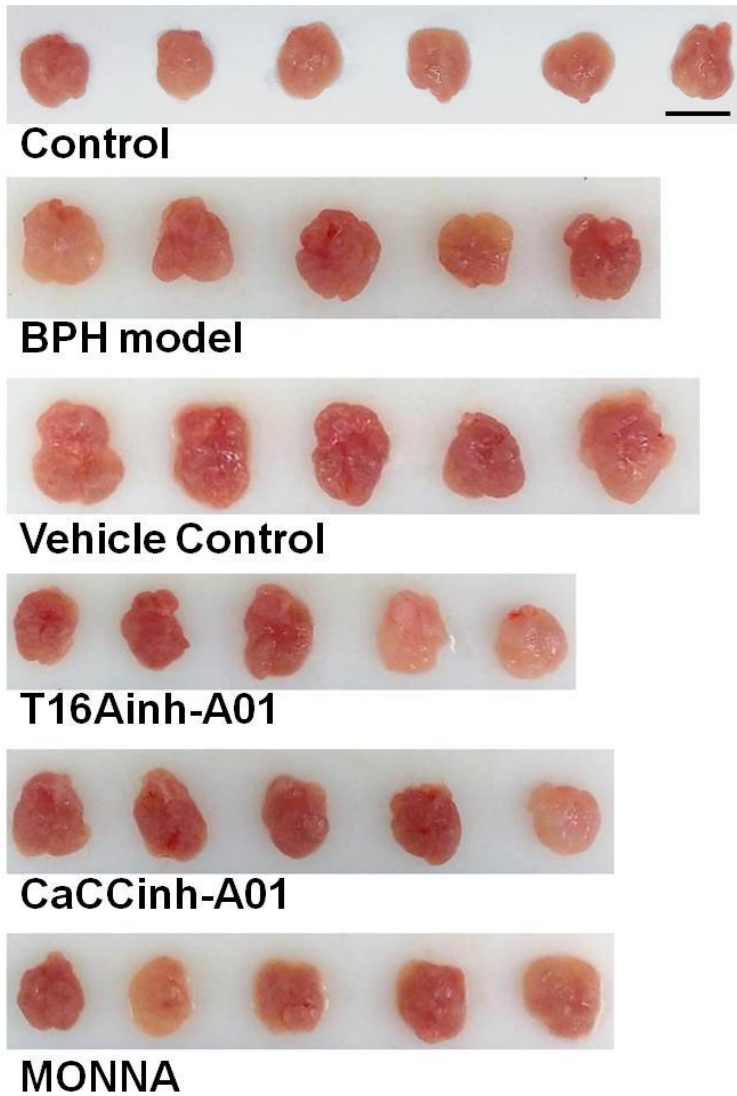

Figure 29. ANO1 inhibitors treated prostate photos of Rat BPH model

Comparison of actual prostate size. Scale bar, 1 cm.

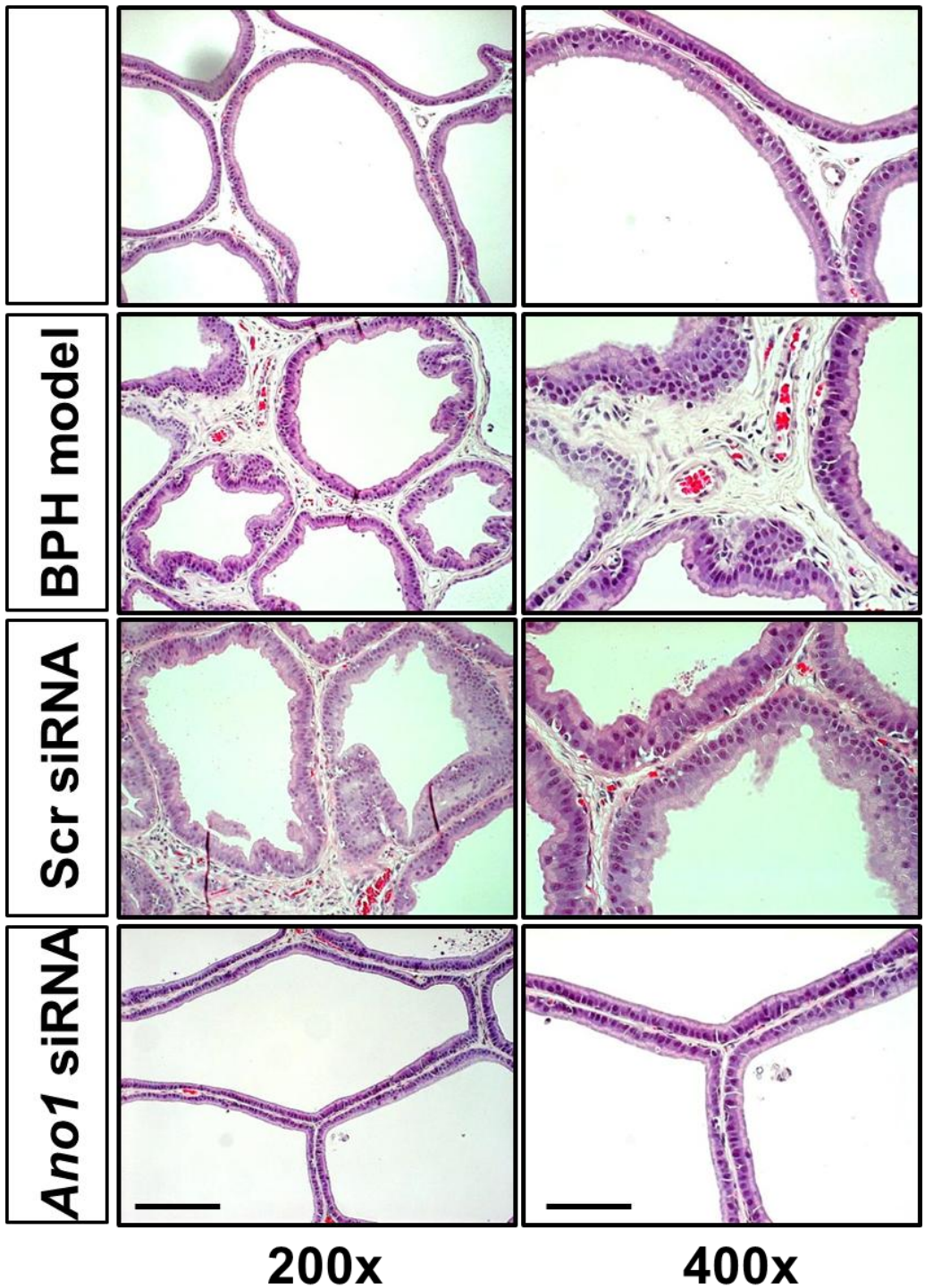
BPH model
Scr siRNA
Ano1 siRNA
200x
400x

Figure 30. Histological analysis of the intraprostatic siRNA injected Rat BPH model

Representative H&E histology of the prostate sections from the rat BPH model. Original magnification, ×200 (left) and ×400 (right). Scale bar, 20 μm.

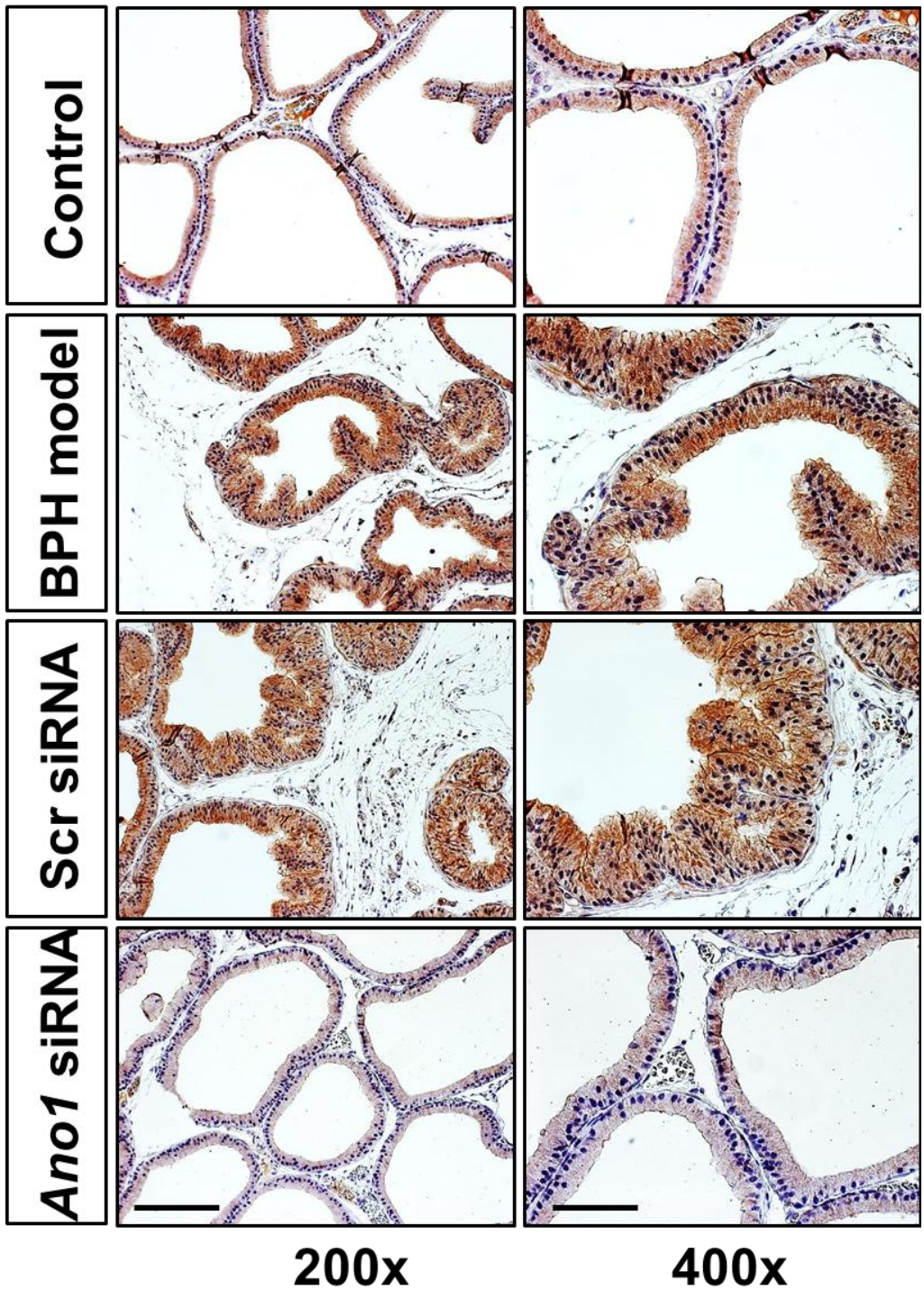
Control
BPH model
Scr siRNA
Ano1 siRNA
200x
400x

Figure 31. ANO1 immunohistochemistry of the intraprostatic siRNA injected Rat BPH model

Representative immunostainings using ANO1 antibody of the prostate sections from the rat BPH model. Original magnification, ×200 (left) and ×400 (right). Scale bar, 20 μm.

11. Intraprostatic injection of Ano1 siRNA suppresses cell proliferation in rat BPH model

To determine whether Ano1 knockdown suppressed cell proliferation in vivo, we examined the expression of specific markers, such as Ki-67 and proliferating cell nuclear antigen (PCNA), in the prostates of BPH-model rats. Treatment with Ano1 siRNA markedly reduced the number of Ki-67-positive cells compared with that in scrambled siRNA-treated BPH-model rats (Fig. 32 A and B) and the level of PCNA (Fig. 33).

The extracellular signal-regulated kinase (ERK) and AKT pathways are main pathways regulating cell proliferation, survival, and differentiation. In addition, ERK and AKT are known to vary with ANO1 expression in prostate and other cancer tissues. Thus, to define the downstream mechanisms underlying the effects of ANO1 on prostate hyperplasia, we performed Western blots in the prostates of BPH-model rats with antibodies of phosphorylated AKT (S473) and ERK (T202/Y204). In addition, because gene ablation of PTEN, a tumor suppressor phosphatase leads to prostate cancer, its expression along with BPH was also determined. The phosphorylation of AKT was markedly increased in BPH prostates compared with those in castration control prostates and completely inhibited by ANO1 knockdown in BPH prostate (Fig. 33 and 34). The level of

phosphorylated ERK was not affected by the change in prostate size. Taken together, these results suggest that Ano1 knock down inhibits cell proliferation in prostates by blocking of AKT phosphorylation.

A

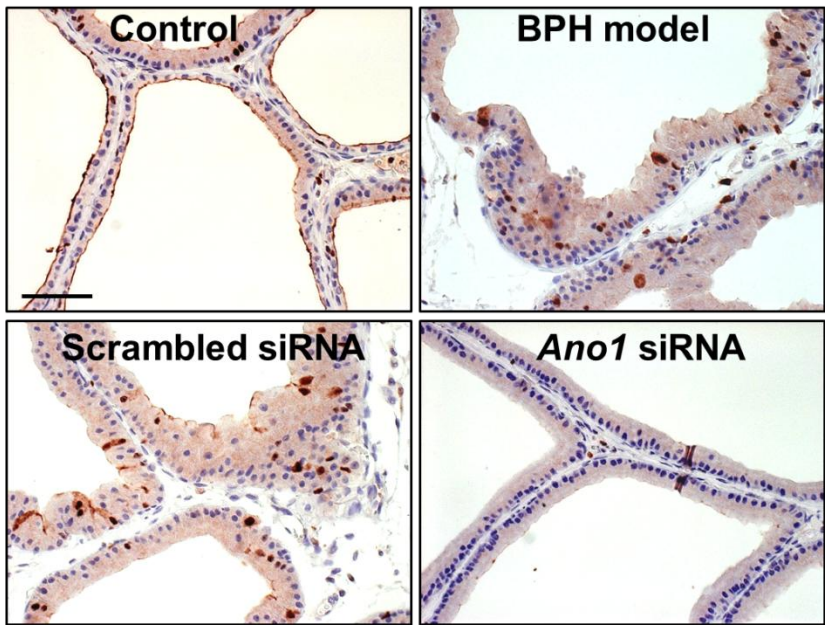
Control
BPH model
Scrambled siRNA
Ano1 siRNA

B

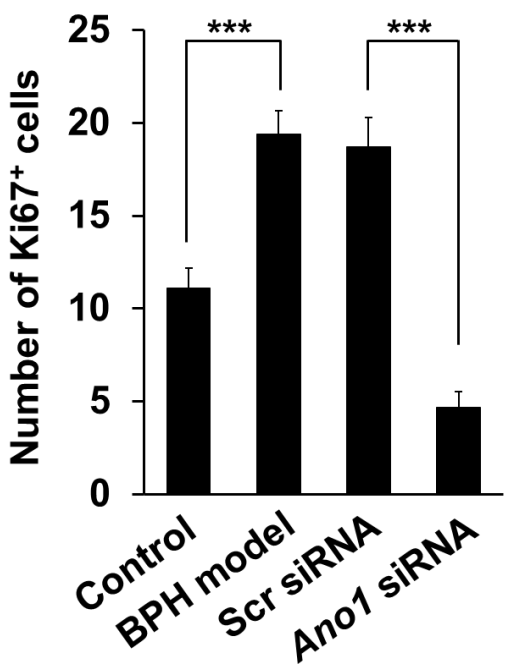
Number of Ki67+ cells
25
20
15
10
5
0
***
***
Control
BPH model
Scr siRNA
Ano1 siRNA

Figure 32. Ki67 immunohistochemistry of the intraprostatic siRNA injected Rat BPH model

(A) Ki-67 immunostaining of paraffin-embedded sections of rat prostates of BPH model and siRNA injected group followed by H&E staining.

(B) The number of Ki-67-positive cells in prostates of control, rat BPH model and BPH model with scrambled or Ano1 siRNA-treated group. ***$p < 0.001$.

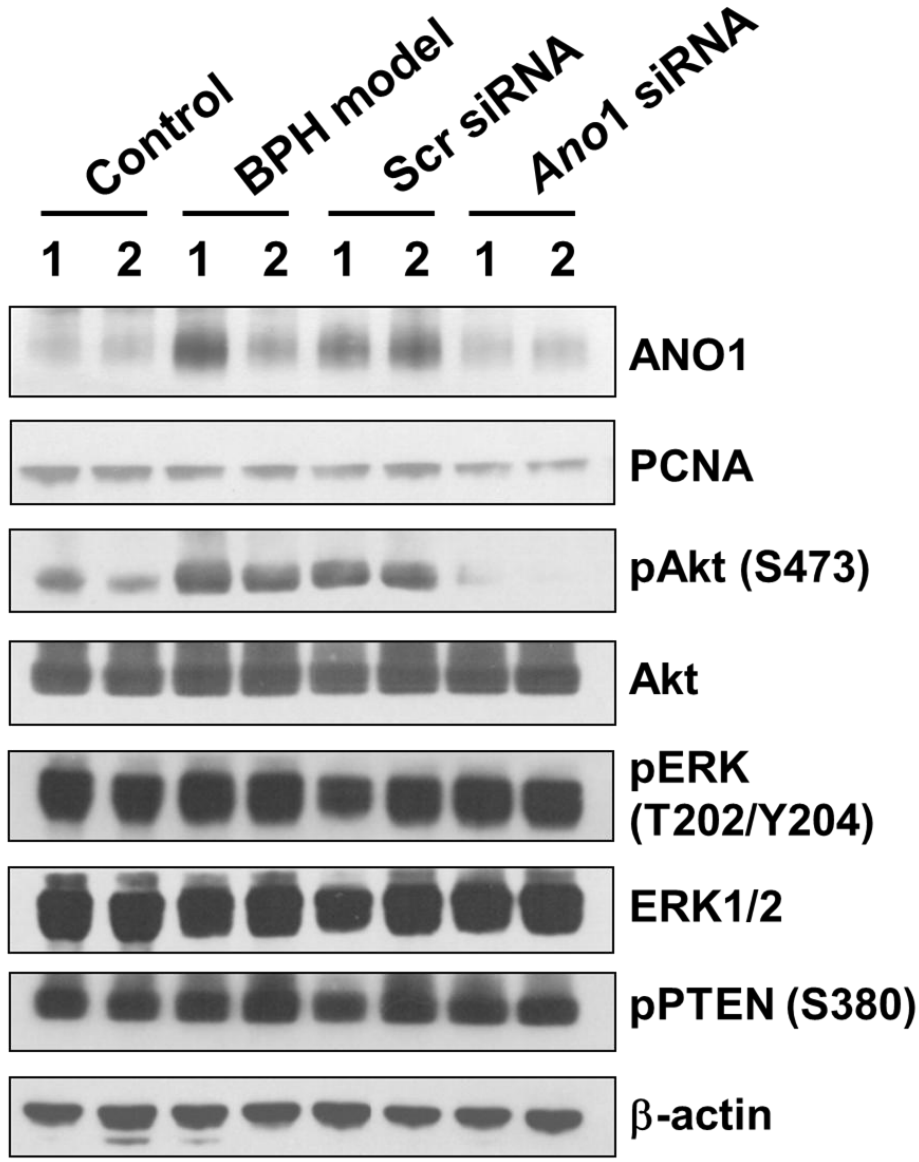
Control
BPH model
Scr siRNA
Ano1 siRNA
1 2 1 2 1 2 1 2
ANO1
PCNA
pAkt (S473)
Akt
pERK (T202/Y204)
ERK1/2
pPTEN (S380)
β-actin

Figure 33. Western Blot analysis of ANO1 downstream in the intraprostatic siRNA injected rat prostates

Immunoblots of ANO1, PCNA, AKT, ERK and phosphorylated PTEN in rat prostate lysates of control, rat BPH model and BPH model with scrambled or Ano1 siRNA-treated group. Phosphorylated AKT (pAKT) and ERK (pERK) were also immunoblotted. The experiments were repeated twice. Numbers above the blots represent the number of experiment. β-actin was used as a control.

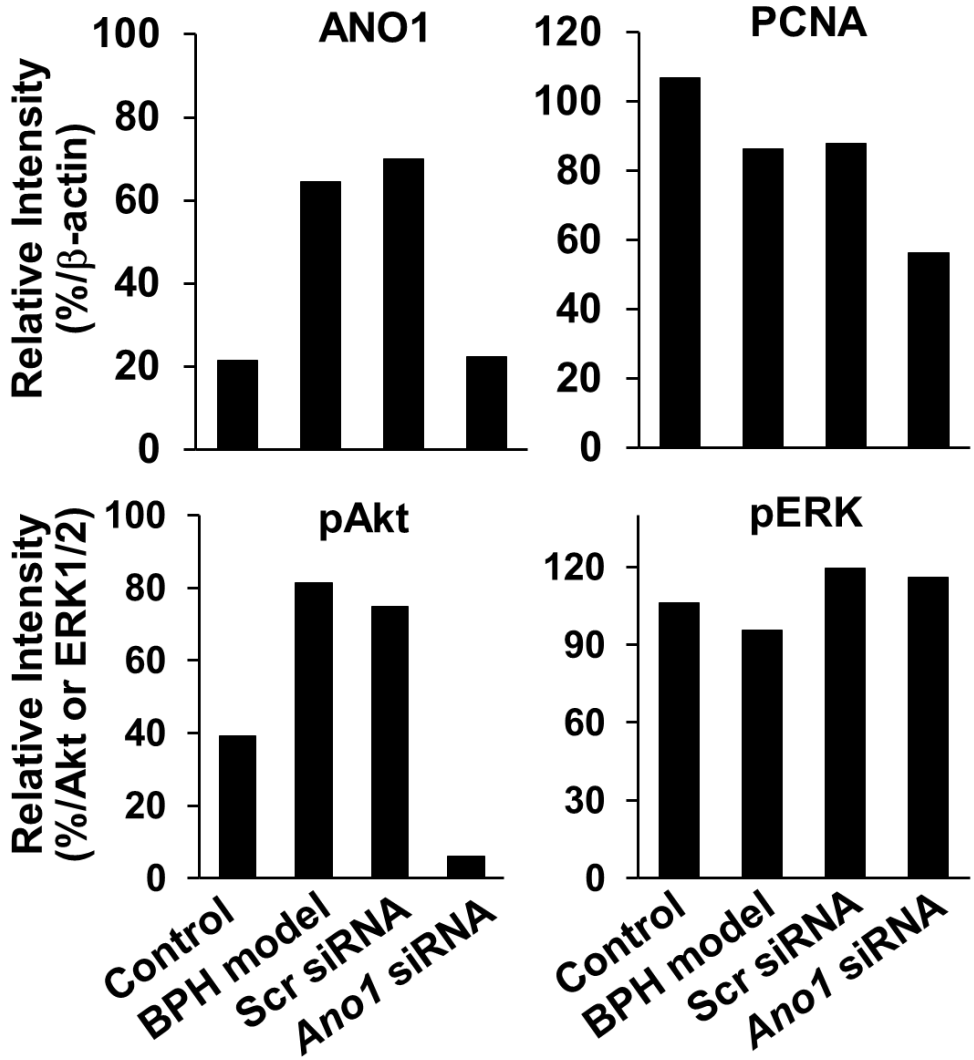

Figure 34. Relative band intensities ANO1, PCNA, pAKT, and pERK

12. ANO1 expression is increased in BPH patient samples

Finally, we investigated whether ANO1 expression is increased in BPH patient samples. Tissue microarray (PR804, Biomax Inc.) was prepared from 70 cases of BPH and 10 cases of prostate adenocarcinoma. Notably, ANO1 immunoreactivity was observed in 36 out of 70 prostate samples (51%) from BPH patients. In addition, among 10 samples from adenocarcinoma prostates 9 samples (90%) were immunoreactive to ANO1 specific antibody (Table 1 and Fig. 35). To further confirm the ANO1 expression in BPH, we also obtained pathological tissue specimens from BPH patients. As shown in Table 1, six out of eight BPH specimens (75%) were positive to ANO1 immunoreactivity. The ANO1 immunoreactivity was found in multilayer-thickening epithelia. These data clearly indicate that human BPH tissues also expressed ANO1.

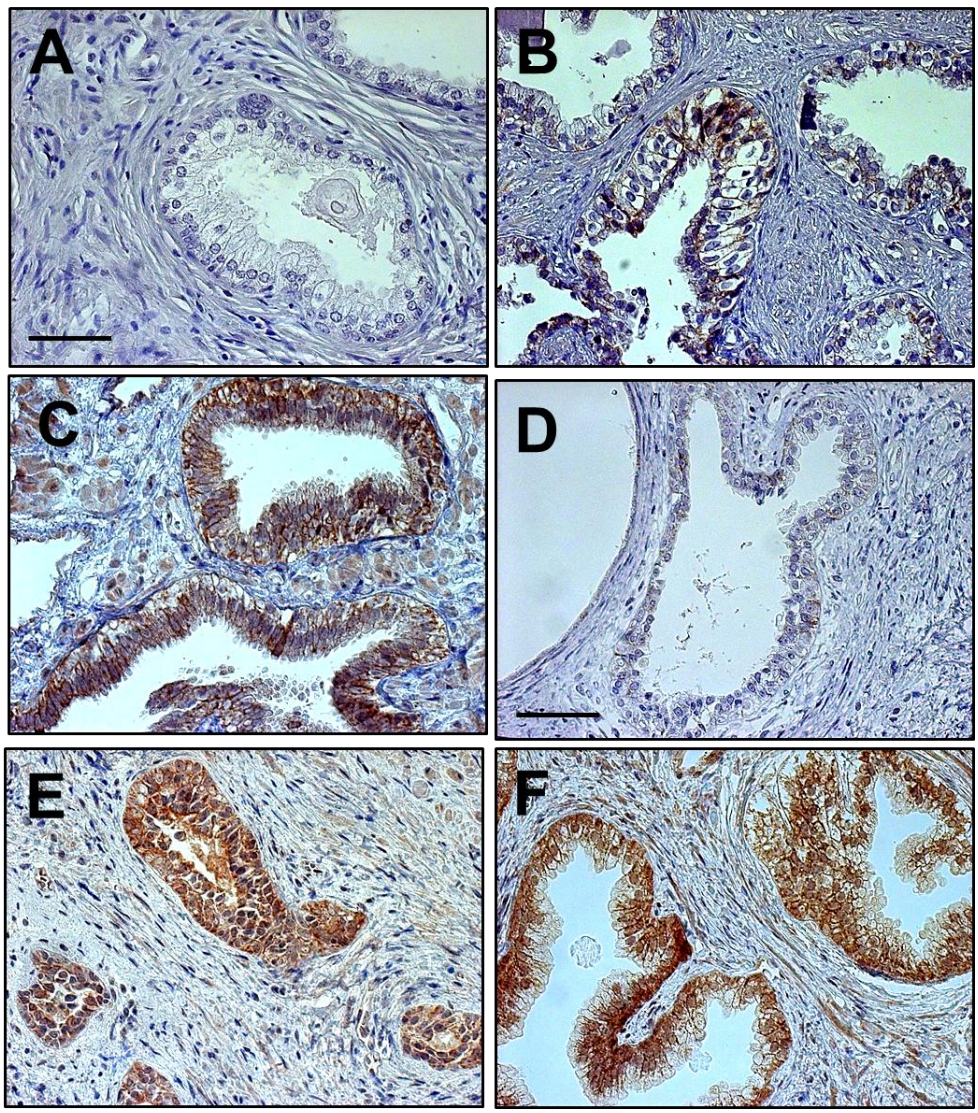
A
B
C
D
E
F

Figure 35. ANO1 immunoshistochemistry of human prostate tissues from BPH and prostate adenocarcinoma

Representative images of ANO1 expression in human hyperplastic prostate samples obtained from tissue microarray (TMA) (PR804, Biomax Inc.) (A-C) and BPH patients (D-F). (A) ANO1 negative control (TMA), (B) prostate from BPH patient (TMA), (C) prostate adenocarcinoma (TMA), (D) negative control, (E, F) BPH patients. Scale bar, 20 μm.

Table 1. Immunohistochemistry analysis of ANO1 expression in human prostate tissues

	Total number of samples	Number of ANO1 positive samples	% ANO1 Positive
Benign Prostatic Hyperplasia (TMA)	70	36	51
Adenocarcinoma (TMA)	10	9	90
Benign Prostatic Hyperplasia (specimens)	8	6	75

Discussion

BPH is characterized by an enlargement of the prostate, which compresses the urethral canal and results in urinary tract obstruction. The major symptoms of BPH are urinary hesitancy, frequent urination, incomplete voiding, and urinary retention leading to renal failure (99). Androgen signaling through the AR is known to play a role in the development of BPH by promoting the proliferation of epithelial or stromal cells (131). The blockage of this signaling can reduce the volume of BPH and relieve the lower urinary tract symptoms (132). Despite the androgen-dependence of hyperplasic cell growth, its downstream signals are still unclear. In this study, we showed that the treatment of prostate epithelial cells with DHT increased endogenous ANO1 expression and enhanced cell proliferation. Because the level of ANO1 was correlated with the concentration of DHT applied to the RWPE-1 cells, ANO1 transcription was suspected to be directly controlled by androgen. Indeed, novel ARE domains were identified in the Ano1 promoter region, by which the expression of ANO1 was controlled transcriptionally through in vivo interaction between the AR and AREs of ANO1 promoter in the presence of

DHT. The application of an ANO1 blocker or ANO1 knock-down suppressed DHT-induced cell proliferation in vitro as well as testosterone-induced prostate cell growth in vivo.

AR downstream signaling is mediated by transcriptional activation when the AR complex binds to the ARE in the promoter regions of target genes. The ARE consensus sequence comprises two 5'-TGTTCT-3' inverted repeats separated by three nucleotides (133). Nucleotide sequencing of the promoter region of Ano1 revealed that the Ano1 promoter contains three putative AREs that had high transcriptional activities in the luciferase reporter assay. ANO1 encodes a CaCC (52-54), and the main function of ANO1 is transepithelial Cl^- secretion. When Cl^- is fluxed out of epithelial cells, water also moves out, resulting in fluid secretion into the lumen. Because ANO1 does not appear to control the cell cycle or mitogenic activity directly, the increased expression of ANO1 in proliferating cells, including tumor cells (91, 93, 94, 117-119), is enigmatic. ANO1 is highly expressed in many types of cancer tissues including prostates (see for review, (123)). The ANO1 amplification is linked to the Ras-ERK pathway in breast cancer or head and neck carcinoma (64, 118). However, the AKT pathway also appears to mediate the ANO1 downstream signals for the cell proliferation in breast cancer cells (118). Consistent with the latter observation, the level of AKT co-varies with cell proliferation in prostates in

the present study. The change in the ERK or AKT level in the ANO1-dependent cell proliferation is largely dependent on the activity of ANO1 as a channel (64, 118). But, how the channel activity of ANO1 is linked to the ERK or AKT pathway is not known. One theory is that the ANO1 activity leads to the increase in intracellular Cl- concentration, which is often found in cancer cells (123). However, when ANO1 is active as a channel, the intracellular concentration of Cl- would decrease, if any, because the Cl- flows out of the cell due to elelctrochemical gradient in epithelial cells. Because depolarization is known to stimulate PI3K/AKT pathway in lung epithelial cells (134), which provides a clue to a missing link between the channel activity of ANO1 and cell proliferation in hyperplastic prostates as well as in cancer cells. Thus, it is likely that the membrane depolarization due to the activity of ANO1 would stimulate the PI3K/Akt pathway, resulting in the cell proliferation. However, this idea needs to be clarified. Because ANO1 mediates the secretion in epithelia as a CaCC (52), the secretion of fluid into the interstitial space via ANO1 could conceivably be advantageous for the proliferative micro-environment. Another hypothesis would be the regulation of cell volume, which is under the control of Cl- channel functions. A volume-regulated anion channel (VRAC) regulates the decrease in volume when a cell is exposed to hypo-osmotic shock (135, 136), and is also known to control the apoptosis-regulated volume (131,

137). Thus, the regulation of cell volume is closely associated with apoptosis. Although ANO1 is not sensitive to hypo-osmotic shock, the activity of ANO1 is probably involved in the control of cell volume, which eventually leads to changes in apoptotic activity.

Several clinical studies have supported the association between BPH and prostate cancer. Prospective and retrospective epidemiologic studies and clinical diagnostic examinations have suggested that BPH is a risk factor for prostate cancer (138, 139). In addition, a 27-year follow-up study suggested a connection between BPH and the incidence of and mortality from prostate cancer (124). In contrast, other studies found a partial association, depending on surgical interventions in BPH patients (140), or no association between BPH and prostate cancer (141, 142). Although no clear evidence of a close relationship between BPH and prostate cancer has been found, they share some common features such as hormone-dependent growth, responses to anti-androgen therapy, and common risk factors such as chronic inflammation, metabolic and genetic factors (126, 127).

Interestingly, ANO1 is also highly expressed in prostate cancer cells and in prostate adenocarcinoma in patients in vivo (119). Thus, regardless of the association between BPH and prostate cancer, ANO1 is expressed both in prostate hyperplasia and cancer cells (119). Because they are susceptible

to androgens that appear to regulate ANO1 expression, unsurprisingly the level of ANO1 has been found to be up-regulated in both diseases. Furthermore, the suppression of ANO1 expression reduces both tumor growth and invasiveness in human prostate carcinoma and the size of the prostate in the BPH model (119). Thus, ANO1 probably plays a key role in the progression of BPH as well as prostate cancer.

In human prostate tissues, Liu and colleagues reported weak or no immunoreactivity in samples from BPH patients compared with the high immunoreactivity in prostate adenocarcinoma (119). In the present study, however, high immunoreactivity was observed in prostate samples from BPH patients (Fig. 32 and Table 1). The inconsistency between the two studies is not clear. However, a small number of BPH samples of previous study may have contributed to the varied results.

In summary, we demonstrated that induction of ANO1 by direct binding of DHT to ARE sites in ANO promoter region is a cause of prostate hyperplasia. Our findings also suggested that pharmacological inhibition of ANO1 decreases cell proliferation and reduces rat prostate size through down-regulation of AKT signaling in BPH development. Most importantly, our findings may shed light on potential opportunities for development of ANO1 specific inhibitors as a therapeutic intervention for BPH patients.

References

1. Verkman AS & Galietta LJ (2009) Chloride channels as drug targets. *Nature reviews. Drug discovery* 8(2):153-171.
2. Gadsby DC, Vergani P, & Csanady L (2006) The ABC protein turned chloride channel whose failure causes cystic fibrosis. *Nature* 440(7083):477-483.
3. Wang SS, *et al.* (2000) Mice lacking renal chloride channel, CLC-5, are a model for Dent's disease, a nephrolithiasis disorder associated with defective receptor-mediated endocytosis. *Human molecular genetics* 9(20):2937-2945.
4. Konrad M, *et al.* (2000) Mutations in the chloride channel gene CLCNKB as a cause of classic Bartter syndrome. *Journal of the American Society of Nephrology : JASN* 11(8):1449-1459.
5. Kasper D, *et al.* (2005) Loss of the chloride channel ClC-7 leads to lysosomal storage disease and neurodegeneration. *The EMBO journal* 24(5):1079-1091.
6. Jentsch TJ, Stein V, Weinreich F, & Zdebik AA (2002) Molecular structure and physiological function of chloride channels. *Physiological reviews* 82(2):503-568.
7. Sheppard DN & Welsh MJ (1999) Structure and function of the CFTR chloride channel. *Physiological reviews* 79(1 Suppl):S23-45.
8. Jentsch TJ, Steinmeyer K, & Schwarz G (1990) Primary structure of Torpedo marmorata chloride channel isolated by expression cloning in Xenopus oocytes. *Nature* 348(6301):510-514.
9. Miller C (1982) Open-state substructure of single chloride channels from Torpedo electroplax. *Philosophical transactions of the Royal Society of London. Series B, Biological sciences* 299(1097):401-411.
10. Matsuda JJ, *et al.* (2008) Overexpression of CLC-3 in HEK293T cells

yields novel currents that are pH dependent. *American journal of physiology. Cell physiology* 294(1):C251-262.

11. Brandt S & Jentsch TJ (1995) ClC-6 and ClC-7 are two novel broadly expressed members of the CLC chloride channel family. *FEBS letters* 377(1):15-20.
12. Neagoe I, Stauber T, Fidzinski P, Bergsdorf EY, & Jentsch TJ (2010) The late endosomal ClC-6 mediates proton/chloride countertransport in heterologous plasma membrane expression. *J Biol Chem* 285(28):21689-21697.
13. Guzman RE, Grieschat M, Fahlke C, & Alekov AK (2013) ClC-3 is an intracellular chloride/proton exchanger with large voltage-dependent nonlinear capacitance. *ACS chemical neuroscience* 4(6):994-1003.
14. Leisle L, Ludwig CF, Wagner FA, Jentsch TJ, & Stauber T (2011) ClC-7 is a slowly voltage-gated 2Cl(-)/1H(+)-exchanger and requires Ostm1 for transport activity. *The EMBO journal* 30(11):2140-2152.
15. Zhang J, Sanguinetti MC, Kwiecinski H, & Ptacek LJ (2000) Mechanism of inverted activation of ClC-1 channels caused by a novel myotonia congenita mutation. *J Biol Chem* 275(4):2999-3005.
16. Piwon N, Gunther W, Schwake M, Bosl MR, & Jentsch TJ (2000) ClC-5 Cl- -channel disruption impairs endocytosis in a mouse model for Dent's disease. *Nature* 408(6810):369-373.
17. Andrini O, *et al.* (2014) CLCNKB mutations causing mild Bartter syndrome profoundly alter the pH and Ca2+ dependence of ClC-Kb channels. *Pflugers Archiv : European journal of physiology* 466(9):1713-1723.
18. Ge YX, Liu Y, Tang HY, Liu XG, & Wang X (2011) ClC-2 contributes to tonic inhibition mediated by alpha5 subunit-containing GABA(A) receptor in experimental temporal lobe epilepsy. *Neuroscience* 186:120-127.
19. Thiagarajah JR & Verkman AS (2003) CFTR pharmacology and its role in intestinal fluid secretion. *Current opinion in pharmacology* 3(6):594-599.

20. Grantham JJ, Chapman AB, & Torres VE (2006) Volume progression in autosomal dominant polycystic kidney disease: the major factor determining clinical outcomes. *Clinical journal of the American Society of Nephrology : CJASN* 1(1):148-157.
21. Pilewski JM & Frizzell RA (1999) Role of CFTR in airway disease. *Physiological reviews* 79(1 Suppl):S215-255.
22. Rommens JM, *et al.* (1989) Identification of the cystic fibrosis gene: chromosome walking and jumping. *Science* 245(4922):1059-1065.
23. Gustafsson JK, *et al.* (2012) Bicarbonate and functional CFTR channel are required for proper mucin secretion and link cystic fibrosis with its mucus phenotype. *The Journal of experimental medicine* 209(7):1263-1272.
24. Ishiguro H, *et al.* (2009) CFTR functions as a bicarbonate channel in pancreatic duct cells. *The Journal of general physiology* 133(3):315-326.
25. Tang L, Fatehi M, & Linsdell P (2009) Mechanism of direct bicarbonate transport by the CFTR anion channel. *Journal of cystic fibrosis : official journal of the European Cystic Fibrosis Society* 8(2):115-121.
26. Kash TL, Trudell JR, & Harrison NL (2004) Structural elements involved in activation of the gamma-aminobutyric acid type A (GABAA) receptor. *Biochemical Society transactions* 32(Pt3):540-546.
27. Hubner CA, *et al.* (2001) Disruption of KCC2 reveals an essential role of K-Cl cotransport already in early synaptic inhibition. *Neuron* 30(2):515-524.
28. Webb TI & Lynch JW (2007) Molecular pharmacology of the glycine receptor chloride channel. *Current pharmaceutical design* 13(23):2350-2367.
29. Johnston GA, Chebib M, Hanrahan JR, & Mewett KN (2003) GABA(C) receptors as drug targets. *Current drug targets. CNS and neurological disorders* 2(4):260-268.
30. Miledi R (1982) A calcium-dependent transient outward current in Xenopus laevis oocytes. *Proceedings of the Royal Society of London.*

Series B, Biological sciences 215(1201):491-497.

31. Bader CR, Bertrand D, & Schwartz EA (1982) Voltage-activated and calcium-activated currents studied in solitary rod inner segments from the salamander retina. *J Physiol* 331:253-284.
32. Tarran R (2004) Regulation of airway surface liquid volume and mucus transport by active ion transport. *Proceedings of the American Thoracic Society* 1(1):42-46.
33. Tarran R, *et al.* (2002) Regulation of murine airway surface liquid volume by CFTR and Ca2+-activated Cl- conductances. *The Journal of general physiology* 120(3):407-418.
34. Stephan AB, *et al.* (2009) ANO2 is the cilial calcium-activated chloride channel that may mediate olfactory amplification. *Proceedings of the National Academy of Sciences of the United States of America* 106(28):11776-11781.
35. Hengl T, *et al.* (2010) Molecular components of signal amplification in olfactory sensory cilia. *Proceedings of the National Academy of Sciences of the United States of America* 107(13):6052-6057.
36. Gonzalez-Silva C, *et al.* (2013) Ca2+-activated Cl- channels of the ClCa family express in the cilia of a subset of rat olfactory sensory neurons. *PloS one* 8(7):e69295.
37. Rasche S, *et al.* (2010) Tmem16b is specifically expressed in the cilia of olfactory sensory neurons. *Chemical senses* 35(3):239-245.
38. Stohr H, *et al.* (2009) TMEM16B, a novel protein with calcium-dependent chloride channel activity, associates with a presynaptic protein complex in photoreceptor terminals. *The Journal of neuroscience : the official journal of the Society for Neuroscience* 29(21):6809-6818.
39. Large WA & Wang Q (1996) Characteristics and physiological role of the Ca(2+)-activated Cl- conductance in smooth muscle. *The American journal of physiology* 271(2 Pt 1):C435-454.
40. Duan D (2009) Phenomics of cardiac chloride channels: the systematic

study of chloride channel function in the heart. *J Physiol* 587(Pt 10):2163-2177.

41. Liu B, *et al.* (2010) The acute nociceptive signals induced by bradykinin in rat sensory neurons are mediated by inhibition of M-type K+ channels and activation of Ca2+-activated Cl- channels. *The Journal of clinical investigation* 120(4):1240-1252.
42. Barrett KE & Keely SJ (2000) Chloride secretion by the intestinal epithelium: molecular basis and regulatory aspects. *Annual review of physiology* 62:535-572.
43. Kachintorn U, Vajanaphanich M, Traynor-Kaplan AE, Dharmsathaphorn K, & Barrett KE (1993) Activation by calcium alone of chloride secretion in T84 epithelial cells. *British journal of pharmacology* 109(2):510-517.
44. Chipperfield AR & Harper AA (2000) Chloride in smooth muscle. *Progress in biophysics and molecular biology* 74(3-5):175-221.
45. Suko Y, Kawahara K, Fukuda Y, & Masuda Y (1997) Nuclear and cytosolic calcium signaling induced by extracellular ATP in rat kidney inner medullary collecting duct cells. *Biochemical and biophysical research communications* 234(1):224-229.
46. Sands JM, *et al.* (1997) Apical extracellular calcium/polyvalent cation-sensing receptor regulates vasopressin-elicited water permeability in rat kidney inner medullary collecting duct. *The Journal of clinical investigation* 99(6):1399-1405.
47. Billet A & Hanrahan JW (2013) The secret life of CFTR as a calcium-activated chloride channel. *The Journal of physiology* 591(Pt 21):5273-5278.
48. Nilius B, *et al.* (1997) Calcium-activated chloride channels in bovine pulmonary artery endothelial cells. *The Journal of physiology* 498 (Pt 2):381-396.
49. Nilius B, *et al.* (1997) Kinetic and pharmacological properties of the calcium-activated chloride-current in macrovascular endothelial cells. *Cell*

calcium 22(1):53-63.

50. Korn SJ, Bolden A, & Horn R (1991) Control of action potentials and Ca2+ influx by the Ca(2+)-dependent chloride current in mouse pituitary cells. *The Journal of physiology* 439:423-437.
51. Lang F, *et al.* (2007) Cell volume regulatory ion channels in cell proliferation and cell death. *Methods in enzymology* 428:209-225.
52. Yang YD, *et al.* (2008) TMEM16A confers receptor-activated calcium-dependent chloride conductance. *Nature* 455(7217):1210-1215.
53. Caputo A, *et al.* (2008) TMEM16A, a membrane protein associated with calcium-dependent chloride channel activity. *Science* 322(5901):590-594.
54. Schroeder BC, Cheng T, Jan YN, & Jan LY (2008) Expression cloning of TMEM16A as a calcium-activated chloride channel subunit. *Cell* 134(6):1019-1029.
55. Milenkovic VM, Brockmann M, Stohr H, Weber BH, & Strauss O (2010) Evolution and functional divergence of the anoctamin family of membrane proteins. *BMC evolutionary biology* 10:319.
56. Hartzell C, Putzier I, & Arreola J (2005) Calcium-activated chloride channels. *Annual review of physiology* 67:719-758.
57. Namkung W, Yao Z, Finkbeiner WE, & Verkman AS (2011) Small-molecule activators of TMEM16A, a calcium-activated chloride channel, stimulate epithelial chloride secretion and intestinal contraction. *FASEB journal : official publication of the Federation of American Societies for Experimental Biology* 25(11):4048-4062.
58. Cho H, *et al.* (2012) The calcium-activated chloride channel anoctamin 1 acts as a heat sensor in nociceptive neurons. *Nature neuroscience* 15(7):1015-1021.
59. Huang F, *et al.* (2012) Calcium-activated chloride channel TMEM16A modulates mucin secretion and airway smooth muscle contraction. *Proceedings of the National Academy of Sciences of the United States of America* 109(40):16354-16359.

60. Lee B, *et al.* (2014) Anoctamin 1 contributes to inflammatory and nerve-injury induced hypersensitivity. *Molecular pain* 10:5.
61. Manoury B, Tamuleviciute A, & Tammaro P (2010) TMEM16A/anoctamin 1 protein mediates calcium-activated chloride currents in pulmonary arterial smooth muscle cells. *The Journal of physiology* 588(Pt 13):2305-2314.
62. Mazzone A, *et al.* (2012) Inhibition of cell proliferation by a selective inhibitor of the Ca(2+)-activated Cl(-) channel, Ano1. *Biochemical and biophysical research communications* 427(2):248-253.
63. Wong XM, Younger S, Peters CJ, Jan YN, & Jan LY (2013) Subdued, a TMEM16 family Ca(2)(+)-activated Cl(-)channel in Drosophila melanogaster with an unexpected role in host defense. *eLife* 2:e00862.
64. Duvvuri U, *et al.* (2012) TMEM16A induces MAPK and contributes directly to tumorigenesis and cancer progression. *Cancer research* 72(13):3270-3281.
65. Adomaviciene A, Smith KJ, Garnett H, & Tammaro P (2013) Putative pore-loops of TMEM16/anoctamin channels affect channel density in cell membranes. *The Journal of physiology* 591(Pt 14):3487-3505.
66. Lee J, *et al.* (2014) Two helices in the third intracellular loop determine anoctamin 1 (TMEM16A) activation by calcium. *Pflugers Archiv : European journal of physiology*.
67. Yu K, Duran C, Qu Z, Cui YY, & Hartzell HC (2012) Explaining calcium-dependent gating of anoctamin-1 chloride channels requires a revised topology. *Circulation research* 110(7):990-999.
68. Terashima H, Picollo A, & Accardi A (2013) Purified TMEM16A is sufficient to form Ca2+-activated Cl- channels. *Proceedings of the National Academy of Sciences of the United States of America* 110(48):19354-19359.
69. Fallah G, *et al.* (2011) TMEM16A(a)/anoctamin-1 shares a homodimeric architecture with CLC chloride channels. *Molecular & cellular proteomics :*

MCP 10(2):M110 004697.

70. Malvezzi M, *et al.* (2013) Ca2+-dependent phospholipid scrambling by a reconstituted TMEM16 ion channel. *Nature communications* 4:2367.
71. Tien J, Lee HY, Minor DL, Jr., Jan YN, & Jan LY (2013) Identification of a dimerization domain in the TMEM16A calcium-activated chloride channel (CaCC). *Proceedings of the National Academy of Sciences of the United States of America* 110(16):6352-6357.
72. Scudieri P, Sondo E, Caci E, Ravazzolo R, & Galietta LJ (2013) TMEM16A-TMEM16B chimaeras to investigate the structure-function relationship of calcium-activated chloride channels. *The Biochemical journal* 452(3):443-455.
73. Schreiber R, *et al.* (2010) Expression and function of epithelial anoctamins. *The Journal of biological chemistry* 285(10):7838-7845.
74. Ousingsawat J, *et al.* (2009) Loss of TMEM16A causes a defect in epithelial Ca2+-dependent chloride transport. *The Journal of biological chemistry* 284(42):28698-28703.
75. Rock JR, *et al.* (2009) Transmembrane protein 16A (TMEM16A) is a Ca2+-regulated Cl- secretory channel in mouse airways. *The Journal of biological chemistry* 284(22):14875-14880.
76. Romanenko VG, *et al.* (2010) Tmem16A encodes the Ca2+-activated Cl- channel in mouse submandibular salivary gland acinar cells. *The Journal of biological chemistry* 285(17):12990-13001.
77. Ousingsawat J, *et al.* (2011) Rotavirus toxin NSP4 induces diarrhea by activation of TMEM16A and inhibition of Na+ absorption. *Pflugers Archiv : European journal of physiology* 461(5):579-589.
78. Dutta AK, *et al.* (2011) Identification and functional characterization of TMEM16A, a Ca2+-activated Cl- channel activated by extracellular nucleotides, in biliary epithelium. *The Journal of biological chemistry* 286(1):766-776.
79. Sagheddu C, *et al.* (2010) Calcium concentration jumps reveal dynamic ion

selectivity of calcium-activated chloride currents in mouse olfactory sensory neurons and TMEM16b-transfected HEK 293T cells. *The Journal of physiology* 588(Pt 21):4189-4204.

80. Pifferi S, Dibattista M, & Menini A (2009) TMEM16B induces chloride currents activated by calcium in mammalian cells. *Pflugers Archiv : European journal of physiology* 458(6):1023-1038.
81. Mercer AJ, *et al.* (2011) Location of release sites and calcium-activated chloride channels relative to calcium channels at the photoreceptor ribbon synapse. *Journal of neurophysiology* 105(1):321-335.
82. Suzuki J, Umeda M, Sims PJ, & Nagata S (2010) Calcium-dependent phospholipid scrambling by TMEM16F. *Nature* 468(7325):834-838.
83. Bera TK, *et al.* (2004) NGEP, a gene encoding a membrane protein detected only in prostate cancer and normal prostate. *Proceedings of the National Academy of Sciences of the United States of America* 101(9):3059-3064.
84. Das S, *et al.* (2007) NGEP, a prostate-specific plasma membrane protein that promotes the association of LNCaP cells. *Cancer research* 67(4):1594-1601.
85. Cereda V, *et al.* (2010) New gene expressed in prostate: a potential target for T cell-mediated prostate cancer immunotherapy. *Cancer immunology, immunotherapy : CII* 59(1):63-71.
86. Williams RM & Naz RK (2010) Novel biomarkers and therapeutic targets for prostate cancer. *Frontiers in bioscience* 2:677-684.
87. Minnerop M & Bauer P (2015) Autosomal recessive cerebellar ataxia 3 due to homozygote c.132dupA mutation within the ANO10 gene. *JAMA neurology* 72(2):238-239.
88. Chamova T, *et al.* (2012) ANO10 c.1150_1151del is a founder mutation causing autosomal recessive cerebellar ataxia in Roma/Gypsies. *Journal of neurology* 259(5):906-911.
89. Vermeer S, *et al.* (2010) Targeted next-generation sequencing of a 12.5 Mb

homozygous region reveals ANO10 mutations in patients with autosomal-recessive cerebellar ataxia. *American journal of human genetics* 87(6):813-819.

90. Hammer C, *et al.* (2015) A coding variant of ANO10, affecting volume regulation of macrophages, is associated with Borrelia seropositivity. *Molecular medicine*.
91. Carles A, *et al.* (2006) Head and neck squamous cell carcinoma transcriptome analysis by comprehensive validated differential display. *Oncogene* 25(12):1821-1831.
92. Espinosa I, *et al.* (2008) A novel monoclonal antibody against DOG1 is a sensitive and specific marker for gastrointestinal stromal tumors. *The American journal of surgical pathology* 32(2):210-218.
93. Huang X, Gollin SM, Raja S, & Godfrey TE (2002) High-resolution mapping of the 11q13 amplicon and identification of a gene, TAOS1, that is amplified and overexpressed in oral cancer cells. *Proceedings of the National Academy of Sciences of the United States of America* 99(17):11369-11374.
94. West RB, *et al.* (2004) The novel marker, DOG1, is expressed ubiquitously in gastrointestinal stromal tumors irrespective of KIT or PDGFRA mutation status. *The American journal of pathology* 165(1):107-113.
95. Ayoub C, *et al.* (2010) ANO1 amplification and expression in HNSCC with a high propensity for future distant metastasis and its functions in HNSCC cell lines. *British journal of cancer* 103(5):715-726.
96. Huang X, Godfrey TE, Gooding WE, McCarty KS, Jr., & Gollin SM (2006) Comprehensive genome and transcriptome analysis of the 11q13 amplicon in human oral cancer and synteny to the 7F5 amplicon in murine oral carcinoma. *Genes, chromosomes & cancer* 45(11):1058-1069.
97. Kunzelmann K (2005) Ion channels and cancer. *The Journal of membrane biology* 205(3):159-173.
98. Berry SJ, Coffey DS, Walsh PC, & Ewing LL (1984) The development of

human benign prostatic hyperplasia with age. *The Journal of urology* 132(3):474-479.

99. Sarma AV & Wei JT (2012) Clinical practice. Benign prostatic hyperplasia and lower urinary tract symptoms. *The New England journal of medicine* 367(3):248-257.

100. Roehrborn CG (2008) Pathology of benign prostatic hyperplasia. *International journal of impotence research* 20 Suppl 3:S11-18.

101. Bartsch G, Rittmaster RS, & Klocker H (2000) Dihydrotestosterone and the concept of 5alpha-reductase inhibition in human benign prostatic hyperplasia. *European urology* 37(4):367-380.

102. Imperato-McGinley J, Guerrero L, Gautier T, & Peterson RE (1974) Steroid 5alpha-reductase deficiency in man: an inherited form of male pseudohermaphroditism. *Science* 186(4170):1213-1215.

103. Huggins C & Clark PJ (1940) Quantitative Studies of Prostatic Secretion : Ii. The Effect of Castration and of Estrogen Injection on the Normal and on the Hyperplastic Prostate Glands of Dogs. *The Journal of experimental medicine* 72(6):747-762.

104. Neuhouser ML, Kristal AR, & Penson DF (2004) Steroid hormones and hormone-related genetic and lifestyle characteristics as risk factors for benign prostatic hyperplasia: review of epidemiologic literature. *Urology* 64(2):201-211.

105. Rohrmann S, Giovannucci E, Smit E, & Platz EA (2007) Association of IGF-1 and IGFBP-3 with lower urinary tract symptoms in the third national health and nutrition examination survey. *The Prostate* 67(15):1693-1698.

106. St Sauver JL, *et al.* (2009) Associations between C-reactive protein and benign prostatic hyperplasia/lower urinary tract symptom outcomes in a population-based cohort. *American journal of epidemiology* 169(11):1281-1290.

107. St Sauver JL, Jacobson DJ, McGree ME, Lieber MM, & Jacobsen SJ (2006)

Protective association between nonsteroidal antiinflammatory drug use and measures of benign prostatic hyperplasia. *American journal of epidemiology* 164(8):760-768.

108. DeCastro J & Stone B (2008) Improving therapeutic outcomes in BPH through diagnosis, treatment and patient compliance. *The American journal of medicine* 121(8 Suppl 2):S27-33.

109. Montorsi F & Mercadante D (2013) Diagnosis of BPH and treatment of LUTS among GPs: a European survey. *International journal of clinical practice* 67(2):114-119.

110. Uno H (1995) [Clinical significance of PSA-density in differential diagnosis between BPH and early stages prostate cancer]. *Nihon Hinyokika Gakkai zasshi. The japanese journal of urology* 86(12):1776-1783.

111. Pascual EM, *et al.* (2011) Usefulness of bladder-prostate ultrasound in the diagnosis of obstruction/hyperactivity in males with BPH. *Archivos espanoles de urologia* 64(9):897-903.

112. Chute CG, *et al.* (1993) The prevalence of prostatism: a population-based survey of urinary symptoms. *The Journal of urology* 150(1):85-89.

113. Gravas S & de la Rosette JJ (2013) Investigational therapies targeted to the treatment of benign prostatic hyperplasia. *Expert opinion on investigational drugs* 22(3):357-368.

114. Carson C, 3rd & Rittmaster R (2003) The role of dihydrotestosterone in benign prostatic hyperplasia. *Urology* 61(4 Suppl 1):2-7.

115. Gur S, Kadowitz PJ, & Hellstrom WJ (2013) Effects of 5-alpha reductase inhibitors on erectile function, sexual desire and ejaculation. *Expert opinion on drug safety* 12(1):81-90.

116. McConnell JD, *et al.* (2003) The long-term effect of doxazosin, finasteride, and combination therapy on the clinical progression of benign prostatic hyperplasia. *The New England journal of medicine* 349(25):2387-2398.

117. Kashyap MK, *et al.* (2009) Genomewide mRNA profiling of esophageal squamous cell carcinoma for identification of cancer biomarkers. *Cancer*

biology & therapy 8(1):36-46.

118. Britschgi A, *et al.* (2013) Calcium-activated chloride channel ANO1 promotes breast cancer progression by activating EGFR and CAMK signaling. *Proceedings of the National Academy of Sciences of the United States of America* 110(11):E1026-1034.
119. Liu W, Lu M, Liu B, Huang Y, & Wang K (2012) Inhibition of Ca(2+)-activated Cl(-) channel ANO1/TMEM16A expression suppresses tumor growth and invasiveness in human prostate carcinoma. *Cancer letters* 326(1):41-51.
120. Stanich JE, *et al.* (2011) Ano1 as a regulator of proliferation. *American journal of physiology. Gastrointestinal and liver physiology* 301(6):G1044-1051.
121. Bill A, *et al.* (2014) Small molecule-facilitated degradation of ANO1 protein: a new targeting approach for anticancer therapeutics. *The Journal of biological chemistry* 289(16):11029-11041.
122. Perez-Cornejo P, *et al.* (2012) Anoctamin 1 (Tmem16A) Ca2+-activated chloride channel stoichiometrically interacts with an ezrin-radixin-moesin network. *Proceedings of the National Academy of Sciences of the United States of America* 109(26):10376-10381.
123. Qu Z, *et al.* (2014) The Ca(2+) -activated Cl(-) channel, ANO1 (TMEM16A), is a double-edged sword in cell proliferation and tumorigenesis. *Cancer medicine* 3(3):453-461.
124. Orsted DD, Bojesen SE, Nielsen SF, & Nordestgaard BG (2011) Association of clinical benign prostate hyperplasia with prostate cancer incidence and mortality revisited: a nationwide cohort study of 3,009,258 men. *European urology* 60(4):691-698.
125. Schenk JM, *et al.* (2011) Association of symptomatic benign prostatic hyperplasia and prostate cancer: results from the prostate cancer prevention trial. *American journal of epidemiology* 173(12):1419-1428.
126. De Nunzio C, *et al.* (2011) The controversial relationship between benign

prostatic hyperplasia and prostate cancer: the role of inflammation. *European urology* 60(1):106-117.

127. De Nunzio C, Aronson W, Freedland SJ, Giovannucci E, & Parsons JK (2012) The correlation between metabolic syndrome and prostatic diseases. *European urology* 61(3):560-570.

128. Bello D, Webber MM, Kleinman HK, Wartinger DD, & Rhim JS (1997) Androgen responsive adult human prostatic epithelial cell lines immortalized by human papillomavirus 18. *Carcinogenesis* 18(6):1215-1223.

129. Nelson PS, *et al.* (2002) The program of androgen-responsive genes in neoplastic prostate epithelium. *Proceedings of the National Academy of Sciences of the United States of America* 99(18):11890-11895.

130. Sonneveld E, Jansen HJ, Riteco JA, Brouwer A, & van der Burg B (2005) Development of androgen- and estrogen-responsive bioassays, members of a panel of human cell line-based highly selective steroid-responsive bioassays. *Toxicological sciences : an official journal of the Society of Toxicology* 83(1):136-148.

131. Okada Y, Sato K, & Numata T (2009) Pathophysiology and puzzles of the volume-sensitive outwardly rectifying anion channel. *The Journal of physiology* 587(Pt 10):2141-2149.

132. Izumi K, Mizokami A, Lin WJ, Lai KP, & Chang C (2013) Androgen receptor roles in the development of benign prostate hyperplasia. *The American journal of pathology* 182(6):1942-1949.

133. Claessens F, *et al.* (2001) Selective DNA binding by the androgen receptor as a mechanism for hormone-specific gene regulation. *The Journal of steroid biochemistry and molecular biology* 76(1-5):23-30.

134. Chatterjee S, *et al.* (2012) Membrane depolarization is the trigger for PI3K/Akt activation and leads to the generation of ROS. *American journal of physiology. Heart and circulatory physiology* 302(1):H105-114.

135. Hoffmann EK, Lambert IH, & Pedersen SF (2009) Physiology of cell

volume regulation in vertebrates. *Physiological reviews* 89(1):193-277.

136. Lang F (2007) Mechanisms and significance of cell volume regulation. *Journal of the American College of Nutrition* 26(5 Suppl):613S-623S.

137. Okada Y, *et al.* (2006) Volume-sensitive chloride channels involved in apoptotic volume decrease and cell death. *The Journal of membrane biology* 209(1):21-29.

138. Hammarsten J & Hogstedt B (2002) Calculated fast-growing benign prostatic hyperplasia--a risk factor for developing clinical prostate cancer. *Scandinavian journal of urology and nephrology* 36(5):330-338.

139. Armenian HK, Lilienfeld AM, Diamond EL, & Bross ID (1974) Relation between benign prostatic hyperplasia and cancer of the prostate. A prospective and retrospective study. *Lancet* 2(7873):115-117.

140. Chokkalingam AP, *et al.* (2003) Prostate carcinoma risk subsequent to diagnosis of benign prostatic hyperplasia: a population-based cohort study in Sweden. *Cancer* 98(8):1727-1734.

141. Greenwald P, Kirmss V, Polan AK, & Dick VS (1974) Cancer of the prostate among men with benign prostatic hyperplasia. *Journal of the National Cancer Institute* 53(2):335-340.

142. Simons BD, Morrison AS, Young RH, & Verhoek-Oftedahl W (1993) The relation of surgery for prostatic hypertrophy to carcinoma of the prostate. *American journal of epidemiology* 138(5):294-300.

국문초록

전립선 비대증은 전립선 크기의 증가로 인한 하부요로증상을 동반하는 질환으로 전세계적으로 고령의 남성에서 매우 높은 비율로 발병하는 것으로 보고되고 있다. 하지만, 아직 전립선 비대증의 발병 과정에 대한 분자생물학적 기전은 명확하게 연구되지 않았다. 칼슘에의해 활성화되는 음이온 채널 (CaCC)인 Anoctamin1 (ANO1)은 인체에서 다양한 생리학적 기능을 매개하는 것으로 최근 보고되었다. 이번 연구에서 우리는 남성 호르몬인 testosterone에 기인한 전립선 비대증에서 ANO1의 역할을 규명하였다. Testosterone의 대사체인 Dihytrotestosterone (DHT)를 처치한 전립선 상피 세포에서 ANO1의 발현이 크게 증가될 뿐 아니라 CaCC 저해제들 또는 ANO1 siRNA를 처치하면 DHT에 기인한 전립선 상피 세포의 증식이 강력하게 억제되는 것을 확인하였다. DHT에 의한 ANO1 발현이 증가되는 기전을 연구한 결과, ANO1의 promoter region에 3개의 Androgen-response elements (AREs)가 존재하는 것을 발견하였고,

DHT 처치에 의존적인 ANO1 증가 및 직접적인 binding을 reporter gene assay와 Chromatin Immunoprecipitation (Chip) assay를 통해 확인하였다. ANO1 선택적 저해제들과 ANO1 siRNA를 Rat 전립선 비대증 동물 모델에서 평가한 결과, 모두 전립선 무게 증가를 유의성 있게 억제시키는 것을 확인하였다. 이상의 결과를 통해, ANO1이 전립선 비대증의 발병에 있어 중요한 역할을 하는 것을 확인하였고, 향후 ANO1 저해제가 전립선 비대증 치료에 유효한 치료 타겟이 될 것으로 기대된다.

키워드: Anoctamin 1 (ANO1), benign prostate hyperplasia (BPH), proliferation